CHAPTER IV

THE SMECTIC A_d-SMECTIC A_2 CRITICAL POINT

4.1 INTRODUCTION

The smectic A phase is characterized by a diffraction pattern which consists of a sharp inner ring (the scattering angle $\theta \sim 1$ to $2°$) and a diffuse outer ring ($8 - 10°$). The inner ring corresponds to the mean thickness of the layer, while the outer ring corresponds to the average distance between the molecules within the plane of the smectic phase. The inner ring is sharp showing that the layer thickness is well defined while the diffuse outer ring signifies that the molecular ordering within a layer is liquid-like. The layer thickness (d) is approximately equal to the length of the molecule (ℓ) (measured in its most extended configuration) when the constituent molecules do not possess a strongly polar group attached to one end. However, when the molecule possesses a strongly polar (cyano or nitro) end group, e.g., 4'-n-octyl-4-cyanobiphenyl (8CB) (see Fig.4.1a), then the layer spacing is generally found to be larger than the length of the molecule. Madhusudana and Chandrasekhar[1] predicted theoretically that in such strongly terminally polar systems, the molecules should be arranged in an antiparallel configuration. A consequence of this antiparallel near neighbour correlation is the formation of a smectic layer whose thickness (d) is greater than the length of the molecule or a bilayer struc-

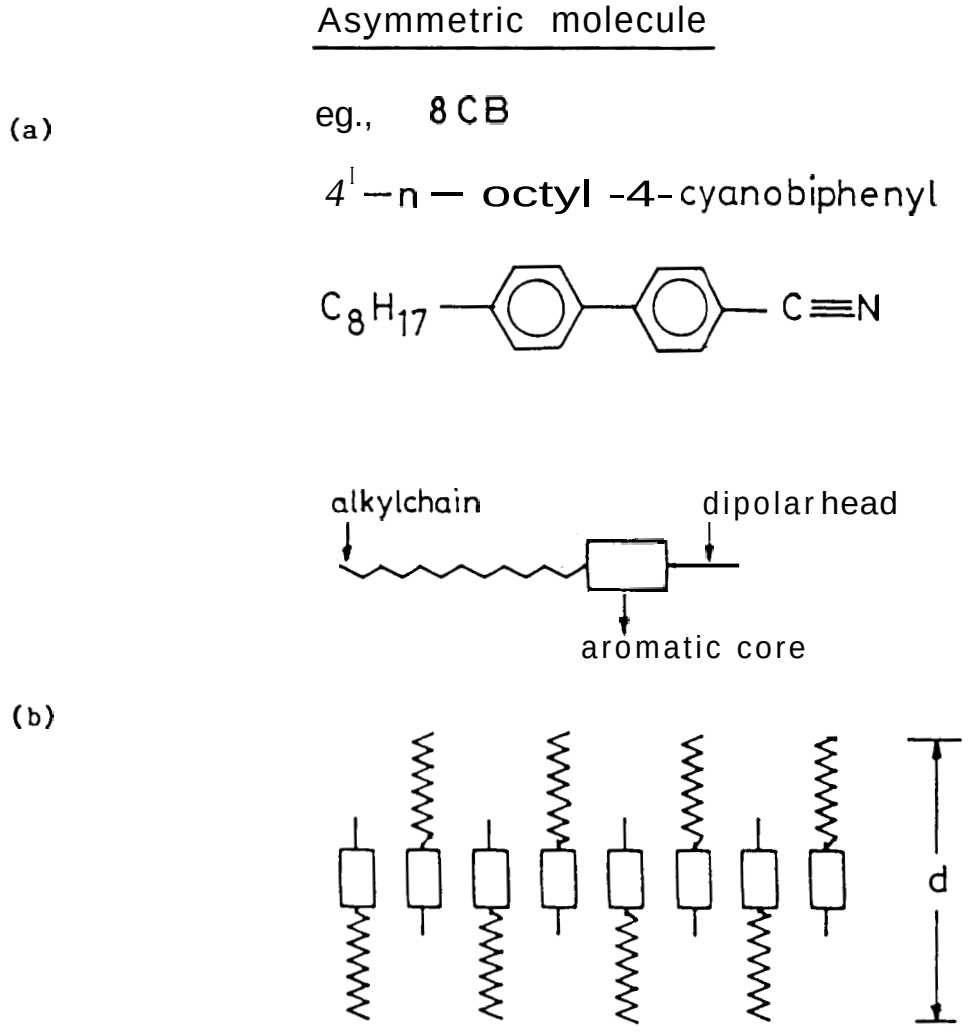

Figure 4.1

(a) Chemical structure of an asymmetric molecule (8CB) and (b) schematic diagram of the molecular arrangement in partially bilayer smectic A phase (A_d) exhibited by strongly polar liquid crystalline materials like, viz., 8CB.

ture (Fig.4.1b). Leadbetter et al[2] showed the existence of such a bilayer structure wherein the aromatic cores overlap in the middle of a layer and the alkyl chains extend outwards. Thus with the synthesis of materials like 8CB it was realized that another type of smectic A phase, viz., the interdigitated type with $d > \ell$ can exist. However, the richness of the variety of smectic A phases was realised only when Sigaud et al.[3] discovered a phase transition between two types of smectic A phases. They found by calorimetry the signature of a phase transition between two polymorphic forms of smectic A phase whose optical textures were identical. Xray studies[4] showed that the diffraction patterns characterising the two types of smectic A phases are distinctly different — that of the high temperature smectic A phase consisted of two reflections which corresponded to $d \approx \ell$ while the low temperature smectic A phase gave a pattern consisting of two pairs of spots corresponding to $d \approx \ell$ and $d \approx 2\ell$. The former was referred to as the monolayer (A_1) phase and the latter as the bilayer (A_2) phase. In this notation the smectic A phase of compounds like 8CB whose layer spacing (d) is such that $\ell < d < 2\ell$ can now be designated as A_d, the partially bilayer phase. Subsequently, three more smectic A phases were discovered. The antiphase[5] or $\tilde{A}$ phase has the basic local symmetry of an A_2 phase, but in addition groups of molecules are arranged with dipolar heads up or down, so that one can look upon the structure as consisting of a 'dipolar wave' within a layer. Another phase called crenelated smectic A

phase (similar to $\tilde{A}$ but with a different symmetry) was discovered by Levelut[6] from Xray experiments. Very recently the incommensurate smectic A phase (A_{ic}) with both A_d-like and A_2-like periodicities was seen by Ratna, Shashidhar and Raja[7]. The existence of such an incommensurate A phase has in fact been predicted theoretically.[8,9] The schematic representation of the molecular arrangement in different polymorphic forms of A are shown in Fig. 4.2.

Perhaps a more realistic description of the smectic A phase is to look upon it as consisting of a density wave in the direction of the director, the periodicity of the modulation giving the smectic layer thickness.[10] (Fig.4.3). Thus the smectic A phase can be looked upon as an orientationally ordered liquid with a one dimensional density wave along the optic axis. The Xray diffraction pattern for such a system gives diffraction spots at a wavevector corresponding to q which is equal to $2\pi/d$, where d is defined as the thickness of the smectic layer. We shall now define Xray diffraction patterns characterising different types of A phases in terms of wavevectors in reciporcal space (see Fig.4.4). The monolayer (A_1) phase exhibits a peak at a wavevector $2q_0 = 2\pi/\ell$. In addition, this phase exhibits diffuse scattering, the nature and position of which depends upon the phase in the neighbourhood of the A_1 phase. Most often this diffuse scattering is centred around a wavevector which is intermediate between q_0 and $2q_0$. The bilayer smectic phase (A_2) is characterised by peaks

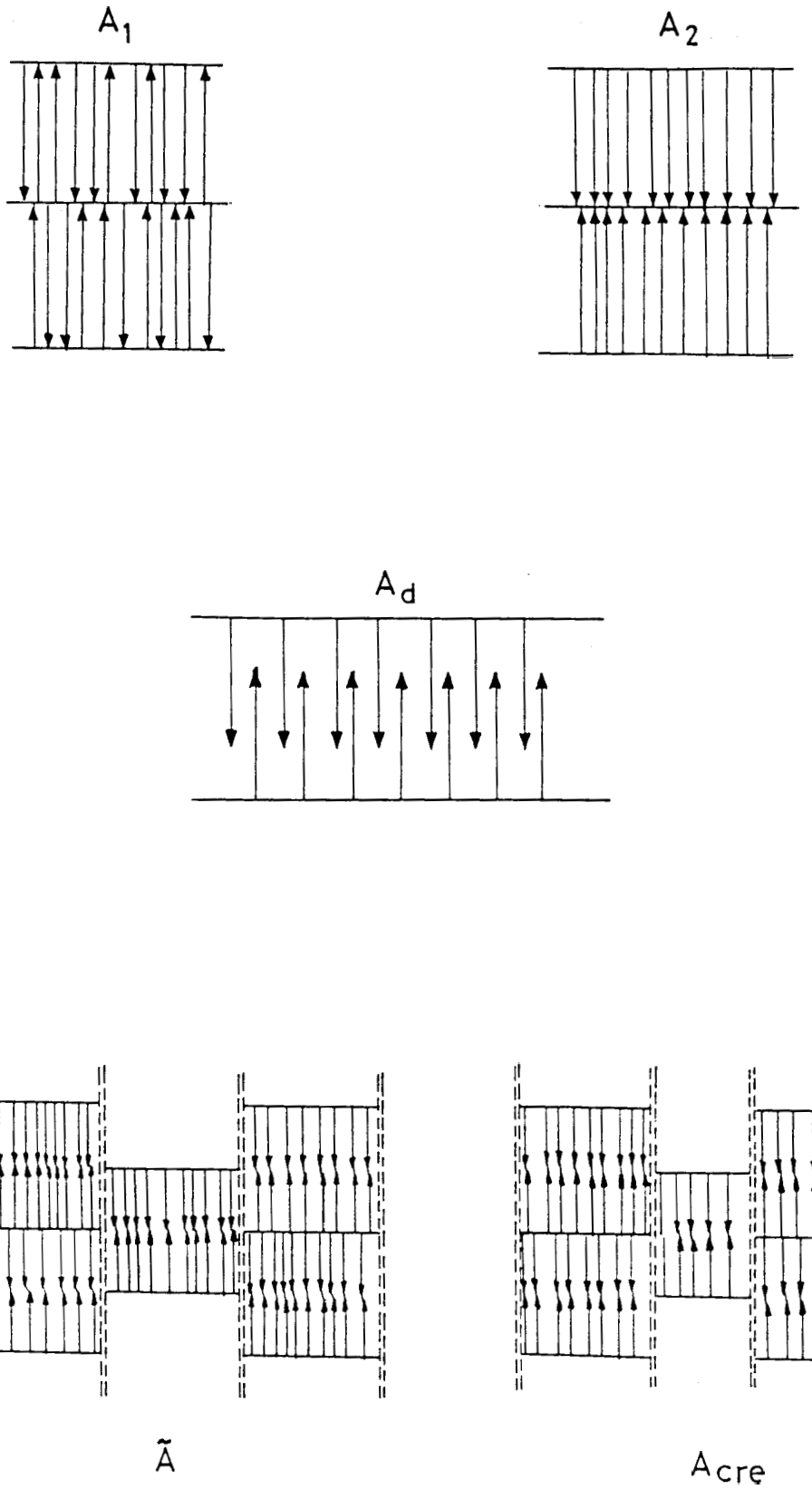

Figure 4.2

Schematic diagram of the molecular arrangement in different smectic A phases.

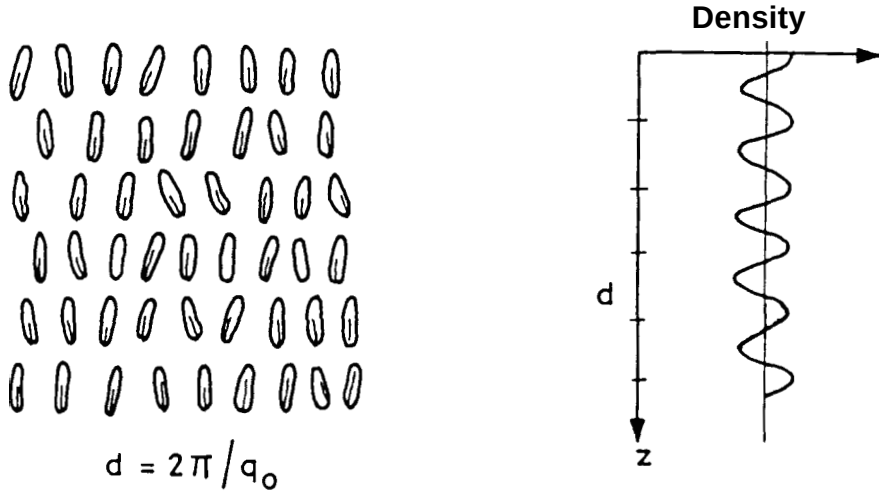

Figure 4.3

Schematic diagram of smectic A phase with its one-dimensional density wave along the average direction of the molecular axis (Ref. 10)

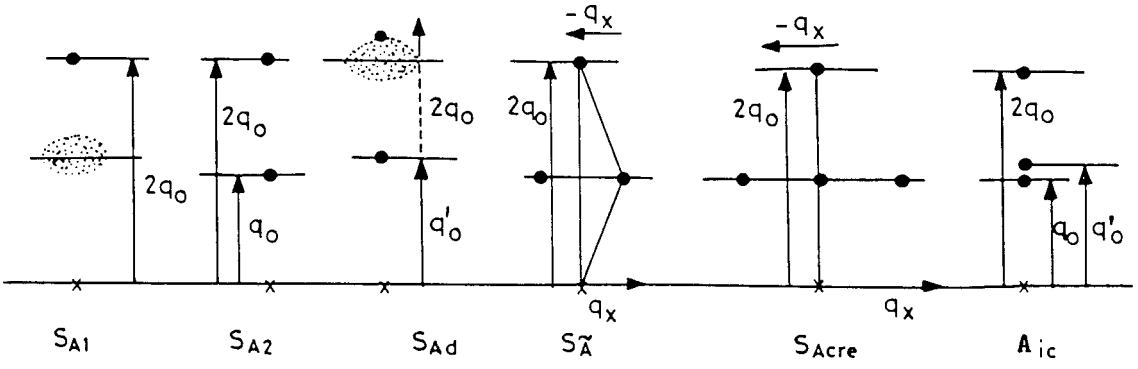

Figure 4.4

Xray diffraction patterns in different smectic A phases. X denotes the loction of the main Xray beam, q_z denotes the equatorial direction, i.e., the direction of the director. The closed circle denotes a condensed Xray reflection while the broad ring indicates a diffuse modulation.

at q_0 and $2q_0$ such that $q_0 = 2\pi/2\ell$ and $2q_0 = 2\pi/\ell$, i.e., corresponding to monolayer and bilayer periodicities, the peak at $2q_0$ being the second harmonic of the one at $q_{0'}$ In the case of A_d phase the condensed Xray reflection is seen at $q_0' = 2\pi/\ell'$, where $\ell < \ell' < 2\ell$ and, generally, a diffuse maximum centred around $2q_{0'}$ In the case of antiphase ($\tilde{A}$) the Xray pattern consists of a spot at $2q_0$ and two spots displaced from Z-axis (optic axis) in a perpendicular direction and situated symmetrically about the q_0 position. This antiphase as well as the recently observed smectic A crenelated phase[6] (A_{cre}) are now known to be biaxial and therefore cannot be truly classified as smectic A phases in the sense we have defined earlier. We shall not be considering these phases in this chapter. The most recently observed incommensurate (A_{ic}) phase has a diffraction pattern characterised by three diffraction spots at q_0, q_0' and $2q_0$, all of them being collinear along the Z-axis (Fig. 4.4).

Most of the above mentioned smectic A polymorphism has been successfully explained in terms of a phenomenological model introduced by Prost and his coworkers.[8,11-13] The nature of the A_d phase and its relation to A_1 and A_2 phases was addressed to theoretically by Barois, Prost and Lubensky.[14] They used the phenomenological model in the framework of the mean field theory to obtain different types of phase diagrams and Xray scattering intensities. In the next section, we shall discuss this theory in some detail and comment

on the predictions of the theory.

4.2 LANDAU THEORY OF FRUSTRATED SMECTICS

As discussed by Prost, two order parameters are required to describe the properties of smectics in which two periodicities are competing with each other. For this reason such smectics have been referred to as **Frustrated Smectics.** The first order parameter $\rho(r)$ is the centre of mass density of constituent molecules. The second order parameter is $P_z(r)$ which describes the long range head to tail configuration of polar molecules along the z-axis (i.e., normal to layers). For the A_1 phase $P_z(r) = 0$, while in the case of A_2 both $\rho(r)$ and $P_z(r)$ have non-zero values. Barois, Prost and Lubensky also find that for certain range of model parameters there can be two bilayer smectic A phases which they have labelled as A_2 and A_2'. In the A_2 phase q_0 the wavevector at which an Xray reflection is seen is of the order of $2\pi/2\ell$ where as in A_2' phase, q is of the order of $2\pi/\ell'$ with $\ell < \ell' < 2R$. Thus the A_2' phase can be identified with the experimentally observed partially bilayer smectic A phase (A_d).

In the absence of competition between the two order parameters $\rho(r)$ would develop spatial modulations along the Z-axis at wavenumber $K_2 = 2\pi/\ell$ where ℓ is of the order of the length of the molecule whereas $P_z(r)$ would describe modulation at $K_1 = 2\pi/\ell'$, where ℓ' is the length associated with a "pair of molecules". To describe the appearance

of modulated order Barois et al. have expressed the order parameters as,

$$P_z(r) = \mathrm{Re}[\psi_1(r)]$$
$$\rho(r) = \mathrm{Re}[\psi_2(r)] \qquad (4.1)$$

where $\psi_1(r)$ and $\psi_2(r)$ are complex fields :

$$\psi_1(r) = \psi_1(r) e^{iq_p \cdot r}$$
$$\psi_2(r) = \psi_2(r)\, e^{iq_\rho \cdot r} \qquad (4.2)$$

In terms of these fields, the Landau-Ginzburg free energy of the model in d-dimensions is

$$\Delta F_s = \int d^d r \, \tfrac{1}{2} r_1 |\psi_1|^2 + \tfrac{1}{2} D_1 |(\Delta + K_1^2)\psi_1|^2 + \tfrac{1}{2} C_1 |\nabla_\perp \psi_1|^2$$
$$+ \tfrac{1}{2} r_2 |\psi_2|^2 + \tfrac{1}{2} D_2 |(\Delta + K_2^2)\psi_2|^2 + \tfrac{1}{2} C_2 |\Delta_\perp \psi_2|^2 + U_1 |\psi_1|^4$$
$$+ U_2 |\psi_2|^4 + 2U_{12} |\psi_1|^2 |\psi_2|^2 - W k e \psi_1^2 \psi_2^*] \qquad (4.3)$$

where $r_1 = a_1(T - T_{1c})$ and $r_2 = a_2(T - T_{2c})$ measure the temperature from the noninteracting mean field transition temperatures T_{1c} and T_{2c} of the fields ψ_1 and ψ_2. $\nabla_\perp$ is a derivative in the plane perpendicular to the z-axis, parallel to n. The $|(\Delta + K_1^2)\psi_1|^2$ and $|(\Delta + K_2^2)\psi_2|^2$ in equation (4.3) favour $q_P^2 = K_1^2$ and $q_\rho^2 = K_2^2$.

To study the mean field phase diagram of linearly modulated

phases they choose q_P and q_P parallel to $n = e_z$ and sought spatially independent fields

$$\psi_1(r) = |\psi_1|$$
$$\psi_2(r) = |\psi_2| \qquad (4.4)$$

which minimize ΔF_s. The following phases were expected:

1) the nematic phase (N) with $|\psi_1| = |\psi_2| = 0$,

2) the monolayer smectic phase (A_1) with $|\psi_1| = 0$ $|\psi_2| \neq 0$, $q_P = K_2$, and

3) the bilayer antiferroelectric smectic phase (A_2) with $|\psi_1| \neq 0$, $|\psi_2| \neq 0$ and $q_P = \frac{1}{2} q_0 = q_0$.

It is to be noted that an antiferroelectric smectic A phase with no long range mass density modulations ($|\psi_1| \neq 0$, $|\psi_2| = 0$) is never stable (see ref. 11) because a non-zero $|\psi_1|$ always generates a non-zero $|\psi_2|$ via the third order term in ΔF_s. In addition, there are antiphases, which will not concern our discussions in this section, in which q_P is not collinear with q_P.[8,15]

The mean field free energy density of the N phase is zero:

$$f_N = 0 \qquad (4.5)$$

The free energy density of the A_1 phase is obtained by minimizing

$$F_{A_1} = (\tfrac{1}{2}) r_2 |\psi_2|^2 + U_2 |\psi_2|^4 \qquad (4.6)$$

with respect to $|\psi_2|$ to yield

$$F_{A_1} = \begin{cases} 0 & r_2 > 0 \\ -\frac{r_2^2}{16U_2} & r_2 < 0 \end{cases} \qquad (4.7)$$

The free energy density of the bilayer A2 phase is obtained by minimizing

$$F_{A_2}(|\psi_1|, |\psi_2|, q_0) = \tfrac{1}{2}[r_1 + D_1(q_0^2 - K_1^2)^2]\,|\psi_1|^2 + \tfrac{1}{2}[r_2 + D_2(4q_0^2 - K_2^2)]\,|\psi_2|^2 - W|\psi_1|^2|\psi_2| + U_1|\psi_1|^4 + U_2|\psi_2|^4 + 2U_{12}|\psi_1|^2|\psi_2|^2 \qquad \ldots . (4.8)$$

with respect to $|\psi_1|$, $|\psi_2|$ and q_o. The minimization with respect to q_o is straightforward, and we obtain

$$q_0^2 \equiv \bar{q}_0^2 = \frac{D_1|\psi_1|^2K_1^2 + 4D_2|\psi_2|^2K_2^2}{D_1|\psi_1|^2 + 16D_2|\psi_2|^2} \qquad (4.9)$$

To proceed with the algebraically complex minimization with respect to $|\psi_1|$ and $|\psi_2|$, they introduced rescaled variables

$$\psi_1 = \frac{2W}{U_{12}}(D_2/D_1)^{1/2} x \cos\theta$$
$$\psi_2 = \frac{1}{2}\frac{W}{U_{12}} x \sin\theta, \qquad (4.10)$$

so that,

$$\bar{\bar{q}}_0^2 = K_1^2\cos^2\theta + \tfrac{1}{4}K_2^2\sin^2\theta \qquad (4.11)$$

x, therefore, measures the degree of order and 8 the relative amplitude of ψ_1 and ψ_2 with small θ corresponding to larger ψ_1. In terms of these variables, the free energy density becomes

$$f(x,\theta) = \frac{U_{12}^3}{W^4}\,\frac{D_1}{D_2}\,f_{A2}(|\psi_1|, |\psi_2|, \bar{\bar{q}}_0^2)$$

$$= x^2(y_1\cos^2\theta + y_2\sin^2\theta + z^2\cos^2\theta\sin^2\theta)$$

$$-2x^3\cos^2\theta\sin\theta + x^4(1+\delta U_1\cos^4\theta + \delta U_2\sin^4\theta), \qquad (4.12)$$

where

$$y_1 = 2\,\frac{U_{12}}{W^2}\,r_1, \quad y_2 = \tfrac{1}{8}\,\frac{D_1}{D_2}\,\frac{U_{12}}{W^2}\,r_2,$$

$$z^2 = \frac{2D_1U_{12}}{W^2}\,(K_1^2 - \tfrac{1}{4}K_2^2)^2, \qquad (4.13)$$

$$\delta U_1 = 16\,\frac{U_1}{U_{12}}\,\frac{D_2}{D_1} - 1, \quad \delta U_2 = \frac{1}{16}\,\frac{U_2}{U_{12}}\,\frac{D_1}{D_2} - 1.$$

y_1 and y_2 are the temperature variables, and z^2 is the <u>incommensurability parameter</u> measuring the degree of mismatch between K_1 and $(\frac{1}{2})K_2$. The usual stability requirements on fourth order terms require $\delta U_{1,2} > -1$. The free energy density now becomes

$$f(x,\theta) = cx^2 + (2/3)bx^3 + (\tfrac{1}{2})ax^4 \qquad (4.14)$$

where $c = y_1 \cos^2\theta + y_2 \sin^2\theta + z^2 \cos^2\theta \sin^2\theta$

$$b = -3\cos^2\theta \sin\theta,$$

$$a = 2(1 + \delta U_1 \cos^4\theta + \delta U_2 \sin^4\theta) \qquad (4.15)$$

Minimizing f with respect to x, they obtained

$$\frac{\partial f(x,\theta)}{\partial x} = 2x(ax^2 + bx + c) = 0 \qquad (4.16)$$

For a given θ, f is a minimum either at $x = \bar{x}(\theta) = 0$ or at $x = \tilde{x}(9) = [\frac{1}{(2a)}][-b + (b^2 - 4ac)^{1/2}]$ when $b^2 - 4ac > 0$. (The smaller root $x = [\frac{I}{(2a)}][-b - (b^2 - 4ac)^{1/2}]$ corresponds to a local maximum of the free energy.) Further they obtained

$$f[\bar{x}(\theta), 0] = 0 \quad \text{for } b^2 < 4ac \qquad (4.17a)$$

$$f[x(\theta), \theta] = [\frac{1}{(12a^3)}]x[-b^4 + b(b^2 - 4ac)^{3/2} + 6ac(b^2 - ac)]$$

$$\text{for } b^2 > 4ac \qquad (4.17b)$$

Finally, Barois et al. performed a nunerical minimization of equation (4.17b) with respect to θ, to locate the solutions corresponding to the lowest free energy. The plots of 'free energy' versus 'θ' are shown in Fig.4.5. We shall now discuss the phase diagrams obtained from the theory.

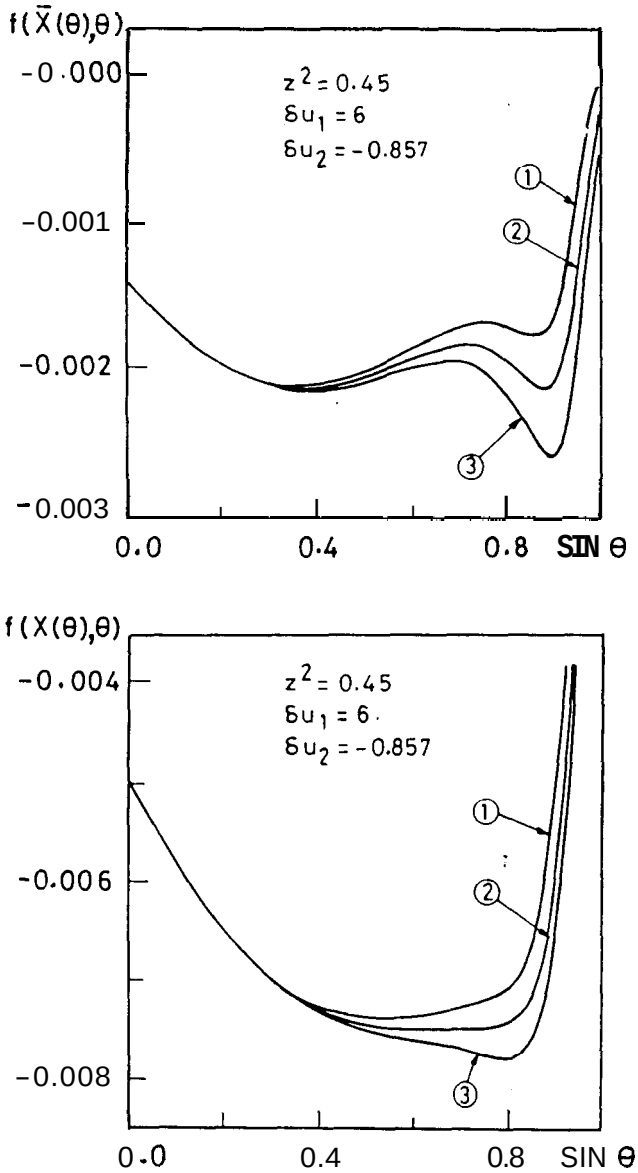

Figure 4.5

Free energy as a function of sin θ, (a) In the strongly first order region and (b) in the vicinity of the critical point. In each figure, there are three curves at constant y_2, but diff'ering y_1. In figure (a) the absolute minimum of curve 1 corresponds to the SA_2' phase and that of curve 3 to the SA_2 phase. Curve 2 with two energetically equivalent minima corresponds to the phase boundary where the SA_2 and SA_2' phases coexist. In figure a, $y_1 = -0.200$, and $y = -0.569 \times 10^{-2}$, -1.069×10^{-2} and -1.569×10^{-2} in curves 1,2 and 3. In figure (b), $y = -0.375$, and $y_2 = +1.520 \times 10^{-3}$, -3.480×10^{-3} and -8.480×10^{-3} for curves 1, 2 and 3 (Ref. 14).

Phase Diagrams

For small incommensurability parameter z^2 and symmetric elastic and fourth order terms ($\delta U_1 = \delta U_2$), the theory predicts a phase diagram shown in Fig.4.6. This diagram predicts the existence of two tricritical points, R and P on both A_1A_2 and NA_2 phase boundaries respectively, both boundaries being first order as they approach N_{A_1} phase boundary. If the elastic constants D_1 and D_2 are different and favour an easy compression of ψ_1 (i.e., δU_1 increases and δU_2 decreases), then, at small values of z^2, a new first order phase boundary separating the A_2 and $A_2'(A_d)$ phases appears. This theoretical phase diagram is shown in Fig.4.7(a). The two phases A_2 and A_2' are distinguished by different values of θ and from equation 4.1 1, different values of $q_{0'}$ For small values of θ, q_0 is of the order of K_1, and ψ_1 is much larger than ψ_2. Therefore the A_2' phase with a small θ can be identified with the experimentally observed A_d phase, although strictly speaking ψ_2 is non zero. For θ intermediate between 0 and $\pi/2$, the amplitudes of ψ_1 and ψ_2 are comparable and this leads to the usual A_2 phase. For the purpose of theoretical description we shall be referring to A_d as A_2' in this section. The discontinuities in $\overline{q_0^2}$ and $\sin^2\theta$ across the new phase boundary are related from equation (4.10), via

$$\Delta\bar{q}_0^2 = (K_2^2/4 - K_1^2)\ \Delta(\sin^2\theta) \qquad (4.18)$$

The new A_2-A_2' phase boundary is tangential to first order N-A_2

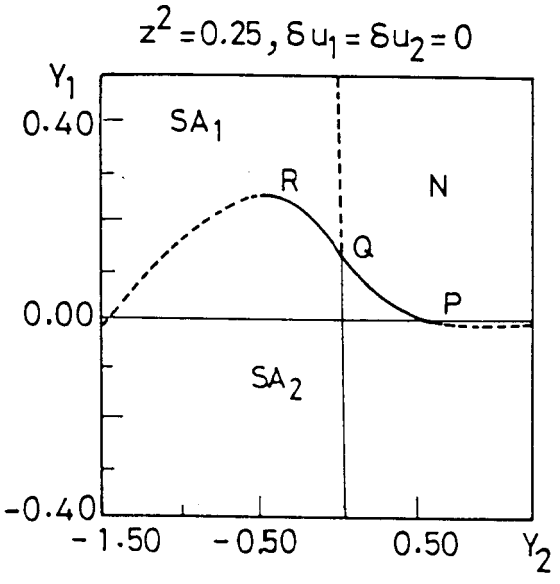

Figure 4.6

Phase diagram in the $y_1 - y_2$ plane for the values of incommensurability parameter $Z^2 = 0.25$ and the potentials $\delta u_1 = \delta u_2 = 0$. Solid (or dashed) lines correspond to first (or second) order transitions (Ref. 14).

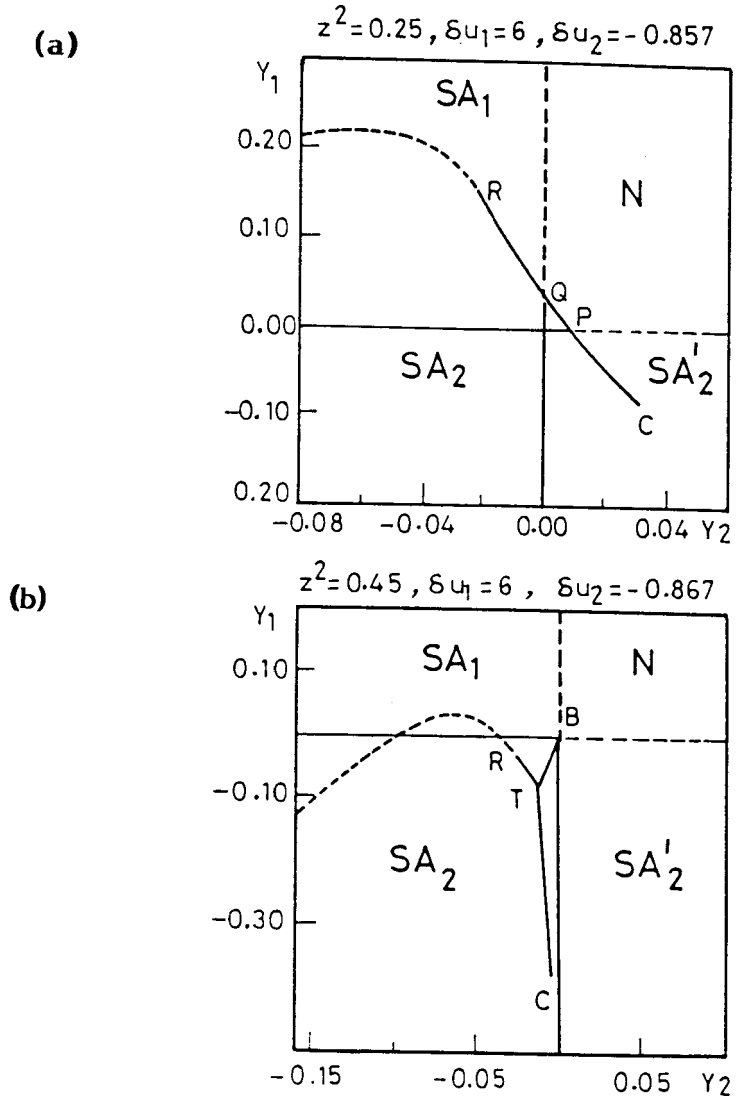

Figure 4.7

Phase diagrams in the $y_1 - y_2$ plane for (a) the incommensurability parameter $Z^2 = 0.25$ and the potentials $\delta u_1 = 6$ and $\delta u_2 = -0.857$. (b) The incommensurability parameter $Z^2 = 0.45$ and the potentials $\delta u_1 = 6$ and $\delta u_2 = -0.857$. (See also legend of Fig. 4.6)(Ref.14).

line at P (Fig.4.7a) and terminates at a critical point c where Δq_0^2 goes to zero. Critical fluctuations similar to the ones encountered at liquid gas critical point are expected in the vicinity of this critical point c. The presence of critical point c indicates that there is no difference in symmetry between A_2 and A_2' phases with different relative amplitudes ψ_1 and ψ_2.

When rhe incommensurability parameter z^2 is further increased or δU_1 increased and δU_2 decreased, the theory predicts a phase diagram shown in Fig.4.7b. In this diagram a new first order $A_2'-A_1$ line is seen which terminates at a mean field bicritical point B (where $N-A_1$ and N-A> lines meet) at one end and at a triple point T at the other end where A,. A_2 and A_2' phases coexist. The critical point c marking the end of the A_2-A_2' boundary continues to exist.

Thus the theory makes several interesting predictions: it predicts a tricritical point for the A_1-A_2 and $N-A_2$ boundaries (Fig.4.6). Recent high resolution Xray studies of Chan et al.[16,17] have shown the existence of a tricritical point on the A_1-A_2 line. These studies have also shown that the Xray correlation length exponents associated with the second order A_1-A_2 transition are isotropic, i.e., $\gamma_{||} = \gamma_{\perp}$. This is indeed expected from theory which predicts that the A_1A_2 transition should belong to the Ising universality class. The $N-A_2$ tricritical point is yet to be observed experimentally. Perhaps the most striking prediction of the theory is concerning the occurrence

of a mean field bicritical point involving N, A_1 and A_2' phases and a critical point, where the first order A_2-A_2' line terminates. Barois et al. have plotted q_0 versus temperature variable y_2 for different values of y_1 in the vicinity of the critical point c (Fig.4.8). This figure is strikingly similar to the P-V (pressure-volume) liquid vapour diagram seen in the vicinity of liquid gas critical point. Although the topological features of some experimental phase diagrams[18] exhibiting the A_1-N_{re}-A_d point were qualitatively similar to those expected near a bicritical point,[14] a high resolution study of the phase diagrams is yet to be carried out. There have been some attempts[19,20] to observe the A_2-A_2' critical point, but so far they have been unsuccessful. We shall summarise in section 4.3 the earlier experiments conducted to observe the A_2-A_2' critical point. This will be followed in §4.4 by a discussion of our results which have led to the first observation of the A_d-A_2 critical point.

4.3 ATTEMPTS TO OBSERVE A_d-A_2 TRANSITION

The first observation of A_d-A_2 transition in a single component system was reported by Hardouin et al.[21] They observed that both the nematic and high temperature smectic A phases of 4-n-heptyl-phenyl-4'-cyanobenzoate (DB7CN) show the coexistence of mass density fluctuations at two incommensurate wavelengths. Although Xray studies clearly showed the existence of A_d and A_2 phases, a detailed study of the layer spacing variation across the A_d-A_2 transition was not

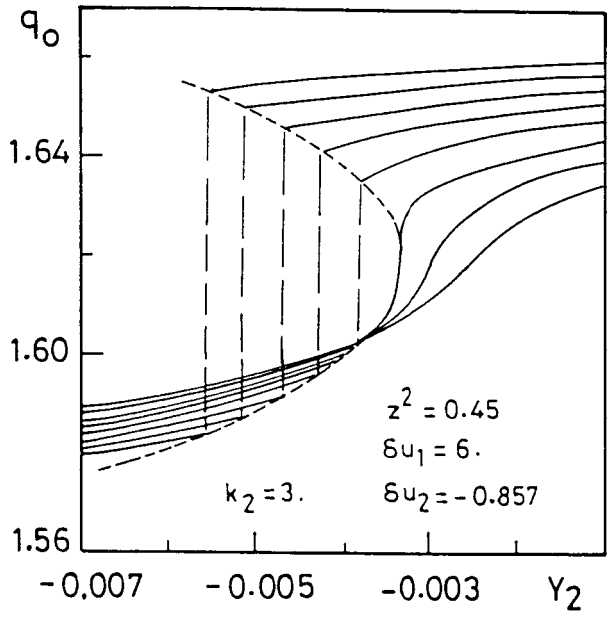

Figure 4.8

Plot of q_0 as a function of y_2 for different y_1. Note the similarity between this diagram and the PV liquid-vapour diagram (Ref. 14).

reported. Recently Hardouin et al.[19] reported Xray studies of the 11th and 12th members of the homologous series, alkyloxy phenyl-4'-(4"-cyanobenzyloxy) benzoate (nOPCBOB), and also a X=0.43 (mol. fraction) binary mixture of 11OPCBOB/12OPCBOB. In another study[20] they reported Xray and differential scanning calorimetric studies of n=7 to 13 members of the homologous series, 4-n-alkyloxyphenyl-4'-(4"-cyanobenzoyloxy)benzoate (DBnOCN). The structural formulae of these systems are shown in Fig.4.9. They observed a strong DSC peak corresponding to the $A_d - A_2$ transition in DB7OCN. With increasing chain length the strength of the DSC peak became weaker until for n=13 member no peak was observed. They also apparently observed from their Xray studies a jump in the layer spacing at $A_d - A_2$ transition for DB7OCN (see Fig.4.10). Such a jump was however not seen for higher members of the series. Essentially a similar result was seen for 11OPCBOB, 12OPCBOB and the y=0.43 (mole fraction) mixture wherein a small jump in layer spacing was seen for 11OPCBOB, but not for 12OPCBOB (4.11). Hardouin et al. concluded that their results suggest a tricritical or critical behaviour for the $A_d - A_2$ transition in the temperature-chain length phase diagram. However, more recently Krishna Prasad et al.[22] carried out precise Xray measurements on DB7OCN and 11OPCBOB. These studies were conducted with a very high accuracy in the determination of wavevectors characterizing the different smectic A phases. The accuracy in the determination of layer spacing in their measurements was 0.05Å while the

DBnOCN Series

4 – n – alkoxyphenyl – 4' – (4'' – cyanobenzoyloxy) benzoate
(n = 7 to 13)

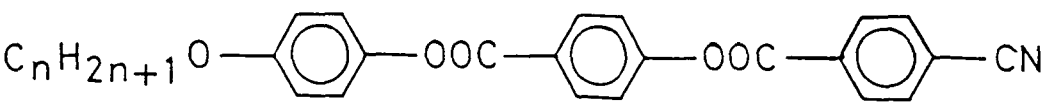

nOPCBOB Series

4 – n – alkoxyphenyl – 4' – (4'' – cyanobenzyloxy) benzoate
(n = 11 and 12)

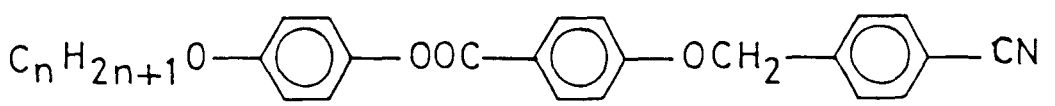

Figure 4.9

Chemical structures of the materials DBnOCN and nOPCBOB series.

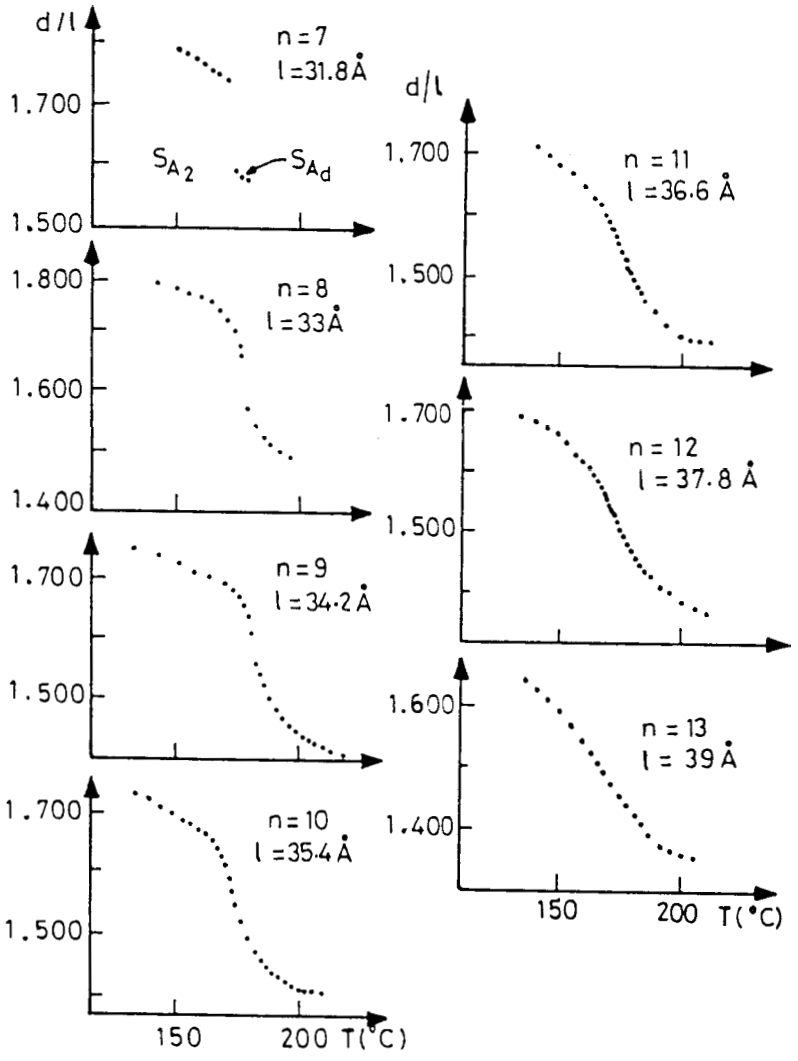

Figure 4.10

Thermal variations of the reduced layer thickness for the DBnOCN series (Ref. 20).

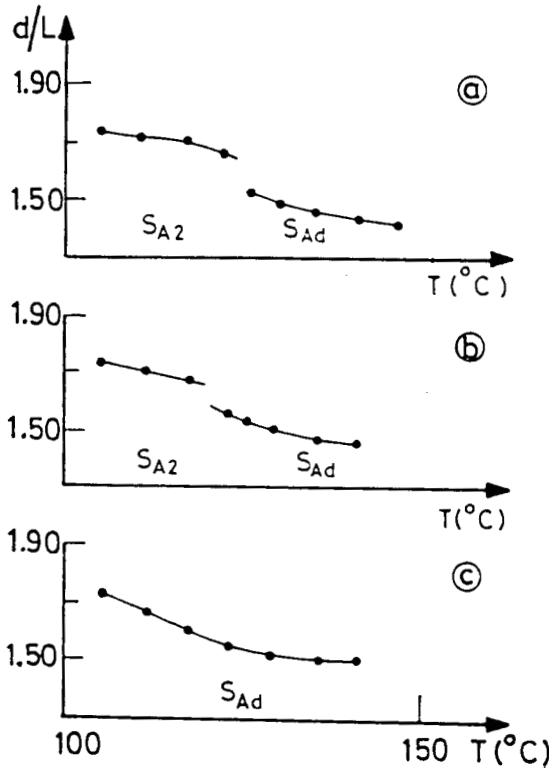

Figure 4.1:

Thermal variation of the reduced layer thickness d/k in 11OPCBOB/12OPCBOB binary mixtures:
(a) 11OPCBOB, ℓ = 36.4 Å, (b) C.43 12OPCBOB in 11OPCBOB, ℓ = 36.9 Å and (c) 12OPCBOB, ℓ = 37.6 Å (From Ref. 20).

temperature constancy was ±10mK during each measurement. Also, Krishna Prasad et al.[22] collected data at very close intervals of temperature in the vicinity of the exepcted A_d-A_2 transition with a view to seeing if there exists a true jump in the layer spacing variation at the A_d-A_2 transition. These studies (shown in Figs. 4.12a and b) clearly showed that there was no jump in the layer spacing at the expected A_d-A_2 transition of either of these materials although the DSC signals clearly showed peaks at the expected transition. (The jump in layer spacing observed by Hardouin et al.[19,20] for the same compounds is perhaps attributable to the fact that they did not have enough data in the vicinity of A_d-A_2 transition.) On the basis of these studies Krishna Prasad et al. concluded that for both DB7OCN and 11OPCBOB there is, in fact, no A_d-A_2 transition and that the A_d phase evolved continuously into the A_2 phase.

Thus all earlier attempts to observe the A_d-A_2 critical point (C.P.) were unsuccessful and it appears that the A_d-A_2 transition itself has probably not been observed conclusively either in a single component system or in mixtures. We shall now describe our studies which resulted not only in a clear observation of such a transition in a binary system, but also led to the observation of a A_d-A_2 critical point. We shall discuss these results in separate sections.

4.4 RESULTS ON MIXTURES OF DB5-90BCB

The constituent compounds are 4-n-pentylphenyl-4'-(4"-cyano-

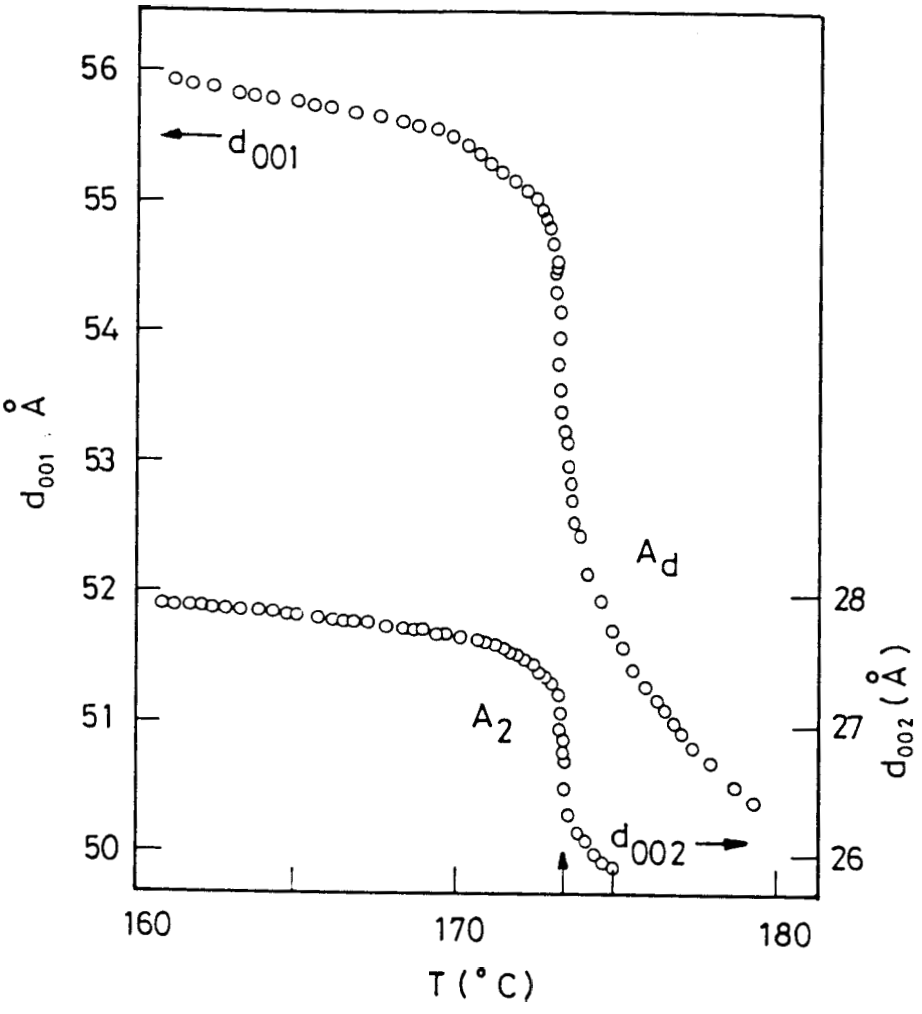

Figure 4.12(a)

Temperature variation of the layer spacing corresponding to (001) and (002) reflections in the A_d and A_2 phases of DB7OCN. The vertical arrow in this figure indicates the temperature at which the $A_d - A_2$ transition is expected from DSC runs (Ref. 22).

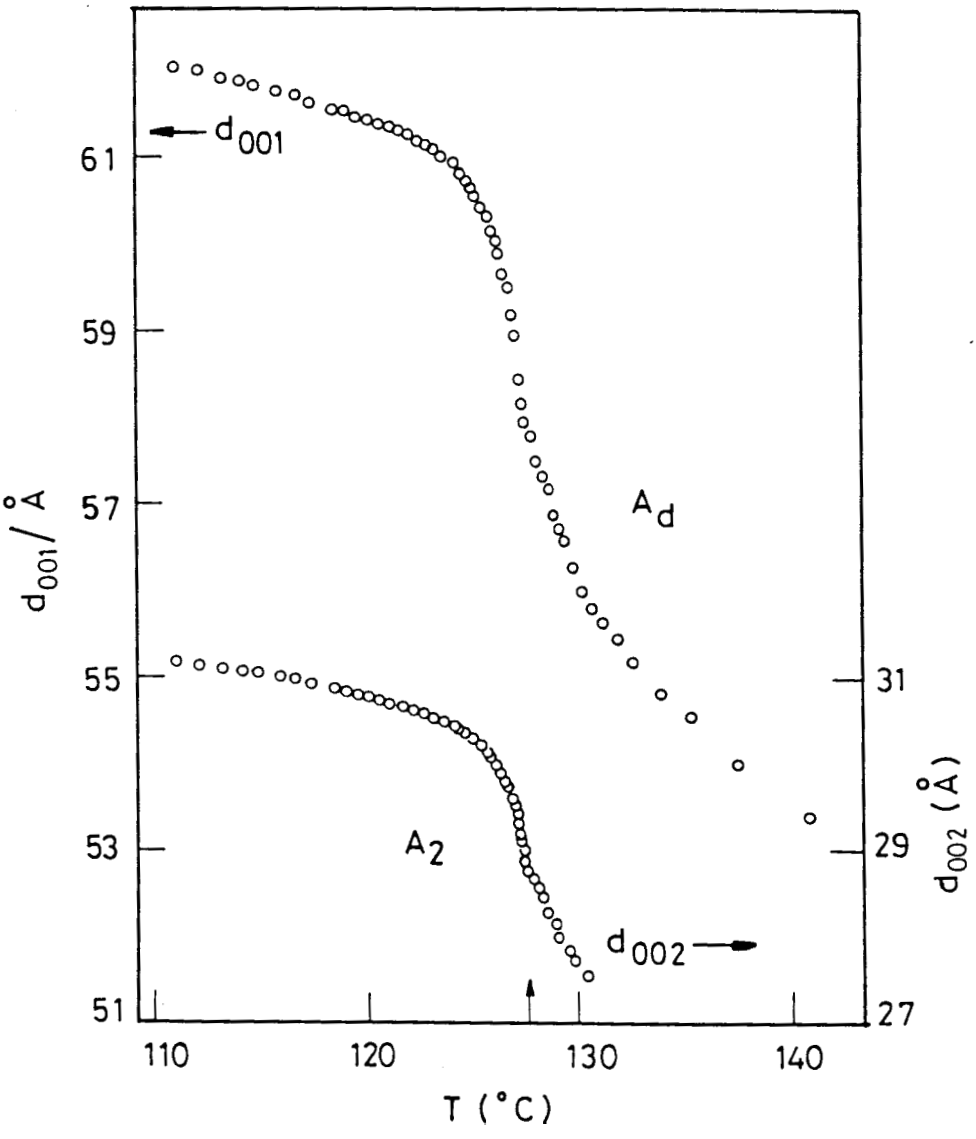

Figure 4.12(b)

Temperature variation of the layer spacing in the A_d and A_2 phases of 11OPCBOB. The vertical arrow indicates the temperature at which the A_d-A_2 transition is expected from DSC runs (Ref. 22).

benzoyloxy)benzoate (DB5) and 4-n-nonyloxybiphenyl-4'-cyanobenzoate (9OBCB) whose chemical structures are shown in Fig.4.13 while their transition temperatures are listed in Table 4.1. The compound 9OBCB exhibits isotropic nematic, A_d and $\tilde{C}$ (ribbon) phases whereas DB5 exhibits isotropic, nematic and A_2 phases. The complete temperature-concentration (T-X) diagram of these systems is given in Fig.4.14. Several interesting features are observed in this phase diagram. They are,

i) an induced smectic A_1 phase is seen over a very narrow range of temperature between A_d and $\tilde{C}$ phases for a concentration range 44-58%.

ii) the $\tilde{C}$ phase is suppressed for concentrations beyond about 59% leading to a direct A_d-A_2 transition.

iii) The A_d-A_2 transition is seen for mixtures with X between 62 and 77 mol %.

iv) the A_d phase itself is suppressed at $x \approx 78\%$ beyond which a direct N-A_2 transition is seen.

v) an induced smectic C (C_2) phase occurs at low temperatures over a concentration range 22-54%. Thus for the concentration range 50-55%, a very rich variety of mesophases are observed on cooling the sample from the isotropic phase, viz., isotropic-nematic-smectic A_d-smectic A_1-$\tilde{C}$-smectic A_2-smectic C (C_2).

DB5

4 – n – pentylphenyl – 4′ – (4″ – cyanobenzoyloxy) benzoate

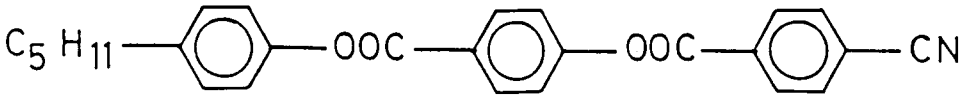

90BCB

4 – n – nonyloxybiphenyl – 4′ – cyanobenzoate

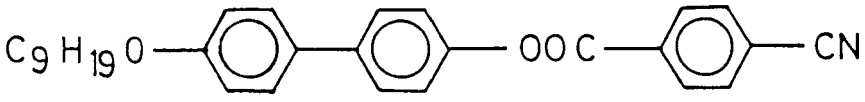

Figure 4.13

Chemical structures of the materials DB5 and 90BCB.

TABLE 4.1

Transition temperatures in °C (at 1 bar) of the compounds

Substance	K	$\tilde{C}$	A_d	N	I
9OBCB		12.6	142.8	207.8	228.3

	K	A_2	N	I
DB5	123.6	140.3	248.1	

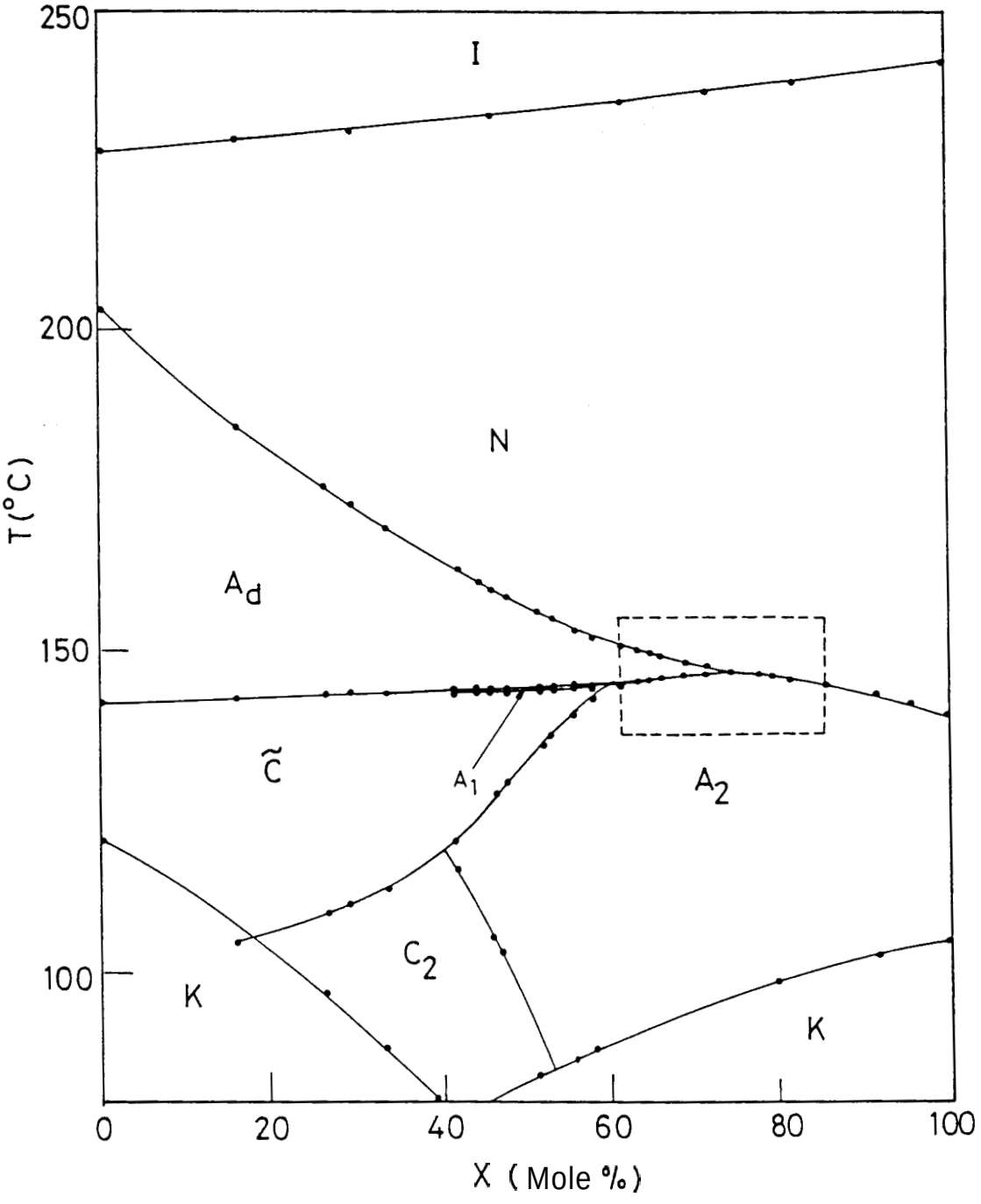

Figure 4.14

Temperature-concentration diagram of DB5/90BCB system. X is mol % of DB5 in the mixture. The part of the phase diagram within the dashed rectangular box is shown in detail in Fig.4.22.

The identification of the different phases was done by Xray diffraction as well as by observation of the optical textures. A typical DSC run showing the signatures of the A_d-A_1 and A_1-$\tilde{C}$ transitions is shown in Fig.4.15. We shall now discuss in detail the results of our Xray studies conducted for two mixtures, viz., 52.6% and 65.6%. (These studies have been conducted using the set-up described in chapter II).

a) **Results** on 52.6% **mixture**

This mixture exhibits the following sequence of transitions on cooling: I-N-A_d-A_1-$\tilde{C}$-A_2-C_2. The sample loaded into a 0.5 mm Lindemann capillary was heated to the nematic phase and cooled slowly (3-4°C/hour) in a magnetic field of ~4 Kgauss to obtain a mono-domain sample of smectic A. The Xray diffraction photographs in different phases (A_d, A_1, $\tilde{C}$ and A_2) are presented in Fig.4.16. The A_d phase is characterised by a pair of condensed spots (4.16a) corresponding to a periodicity $q = 2\pi/\ell'$, where $\ell < \ell' < 2\ell$. On approaching the $\tilde{C}$ phase suddenly A_1 phase appears (Fig.4.16b) whose characteristic diffraction pattern consists of condensed spots at $2q_0$. The layer spacing corresponding to the pair of reflections is 26.7 Å while the length of molecule as measured for this concentration is 28.6 Å showing thereby that this is the A_1 phase. The picture in Fig.4.16b also shows very weak diffuse scattering at low wavevectors (d ~ 50 Å). The complete analysis of this diffuse scattering was not possible

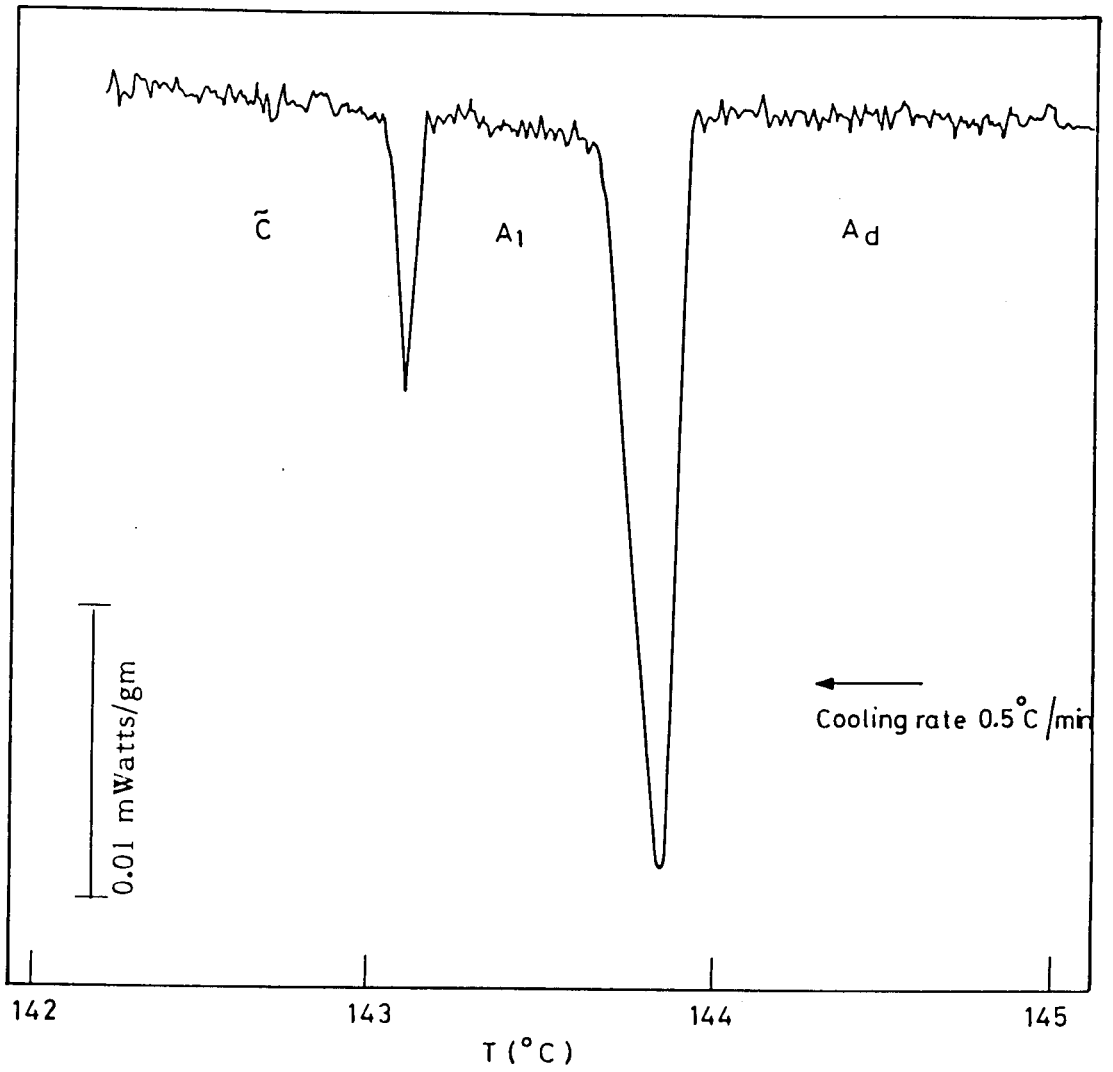

Figure 4.15. DSC runs for 44% DB5 mixture showing an induced A_1 phase between A_d and $\tilde{C}$ phases.

a) A_d phase (144°C)

b) A_1 phase (143.5°C)

c) $\tilde{C}$ phase (142.6°C)

d) A_2 phase (136°C)

Figure 4.16

Photographs showing the Xray diffraction spots corresponding to A_d, A_1, $\tilde{C}$, and A_2 phases exhibited by 52.6% DB5/90BCAB mixture.

because of the very weak nature of the diffuse reflections and also because of the experimental difficulties involved owing to the fact that the smectic A_1 phase exists only over a very narrow range of temperature ($\sim 0.7°C$). On further cooling a clear signature of the ribbon phase ($\tilde{C}$) is seen (Fig.4.16c). The feature of the $\tilde{C}$ phase diffraction pattern is the non uniform intensity of spots which are locted off the Z-axis. Decreasing the temperature further, a diffraction pattern (Fig.4.16d) with two pairs of condensed spots is obtained wherein each of the pairs of spots corresponds to $q_0 = 2\pi/\ell$ and $2q_0 = 2\pi/\ell$ respectively, showing thereby the bilayer nature of the smectic phase (A_2). On further cooling, C_2 phase was found which essentially had diffraction pattern same as that for A_2 phase but with lower layer spacing values (indicating the tilt of molecules). The variation of layer spacing with temperature is shown in Fig.4.17. d exhibits a steep increase in the A_d phase on approaching the A_1 phase.

b) **Results** on 65.6% **mixture**

The Xray data for this mixture have been collected using the photographic set up as well as computer controlled Huber Xray Diffractometer (see Chapter II). On cooling the sample from nematic phase, the smectic A_d phase is seen as characterized by the diffraction pattern shown in figure 4.18a. Cooling further A_2 phase is formed (Fig.4.18b). The transition between A_d and A_2 phases was seen optically as a readjustment of focal conics. But the most important evi-

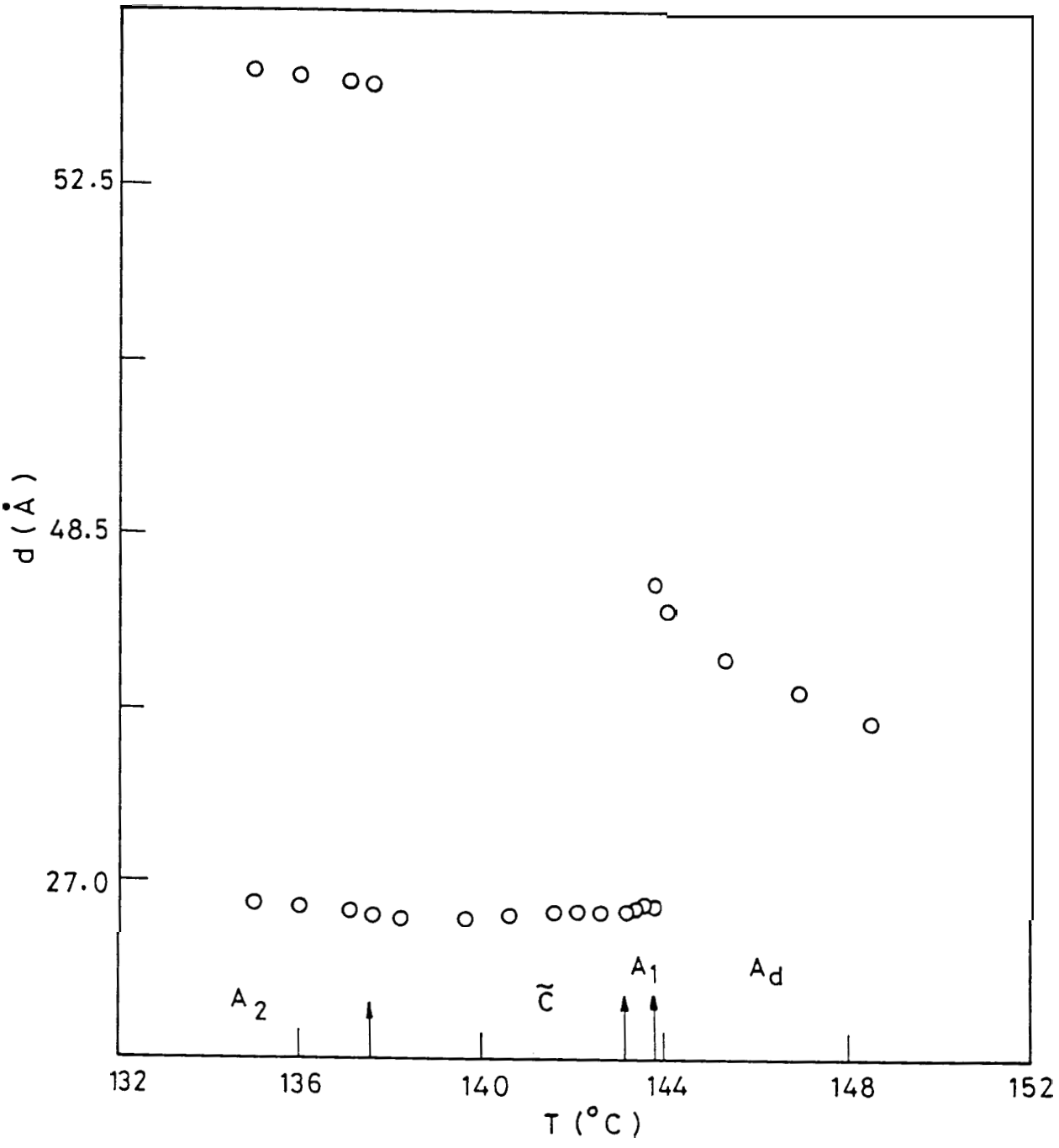

Figure 4.17

Temperature varition of layer spacing in A_d, A_1, $\tilde{C}$ and A_2 phases for (001) aod (002) reflections for X = 52.6% mixture of DB5.

(a) A_d phase (t = 147.1°C)

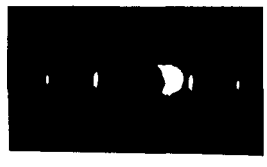

(b) A_2 phase (t = 145.2°C)

Figure 4.18

Photographs showing the Xray diffraction spots in A_d and A_2 phases of 65.6% DB5/9OBCB mixture.

dence for the existence of A_d-A_2 transition comes from the accurate data given in Fig.4.19 which gives variation of layer spacing corresponding to the fundamental reflections in the A_d and A_2 phases (i.e., q_0 in A_2 and q_0' in A_d phase), on cooling the sample from A_d to A_2 phase. It is seen that in the A_d phase the layer spacing increases with decrease in temperature. The signature of the A_d-A_2 transition is a small two phase region (~350 mK) in which the modulations corresponding to both the A_d and A_2 phases coexist. This is as expected and indeed seen for an earlier[23] for a first order transition between two smectic phases of different periodicities. One can associate a jump in layer spacing of about 2.6 Å at the A_d-A_2 transition. Such a strong and clear signature of A_d-A_2 transition is also expected from theoretical considerations. An essentially similar behaviour is seen for the layer spacing variation corresponding to the second harmonic reflections $2q_0$ and $2q_0'$ (Fig.4.20). Fig.4.21 shows a DSC run for 65.6% mixture where A_d-A_2 transition is characterized by a strong sharp signal. Thus the existence of first order A_d-A_2 transition for 65.6% DB5 mixture is clearly established.

Essentially similar behaviour was seen for all the concentrations in the range 64% to 72%, the range over which A_d-A_2 transition was seen. There was no marked decrease in the jump for layer spacing at any of these concentrations and hence a critical point for A_d-A_2 boundary was not observed. This was probably because of reduction

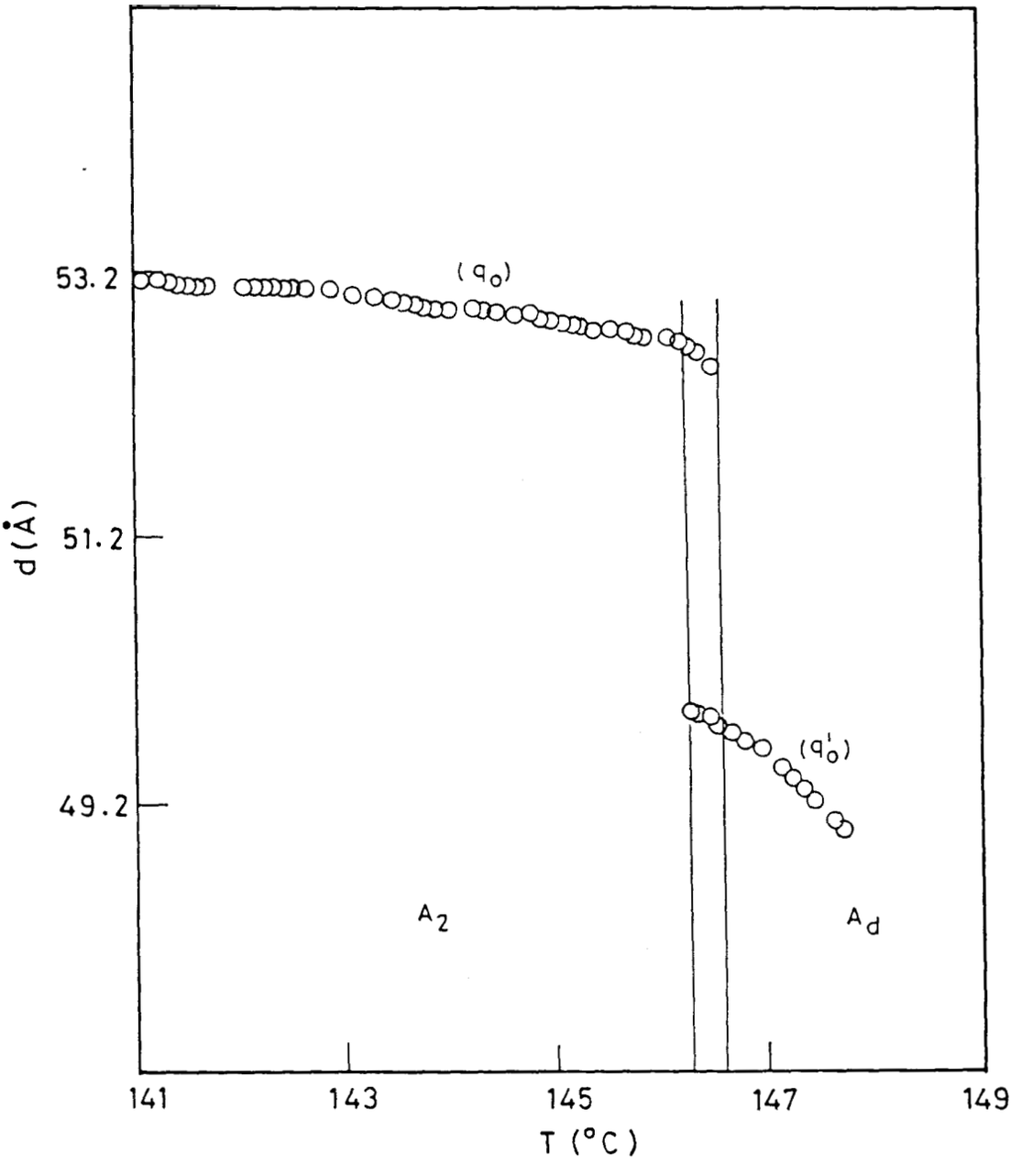

Figure 4.19

Temperature variation of layer spacing corresponding to (001) reflections in the A_d and A_2 phases of 65.6% DB5 mixture. The region between the vertical lines is the two-phase region wherein the density modulations of both the A_d and A_2 phases coexist.

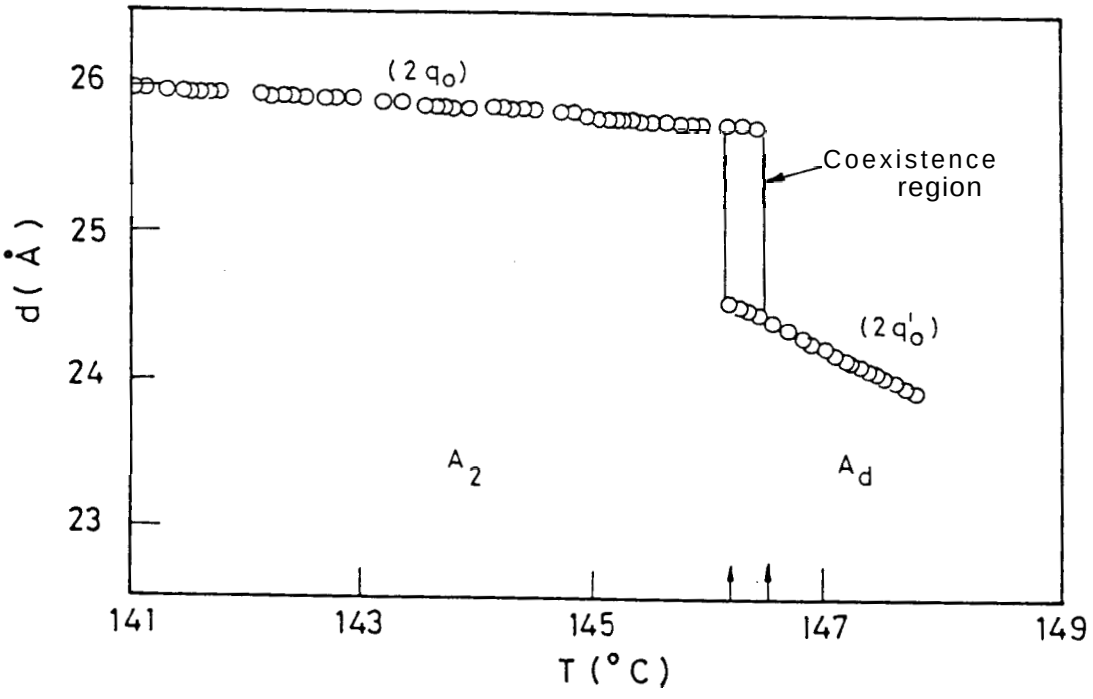

Figure 4.20

Thermal variation of d_{002} in A_d and A_2 phases of X = 65.6 mol.% of mixture of DB_5

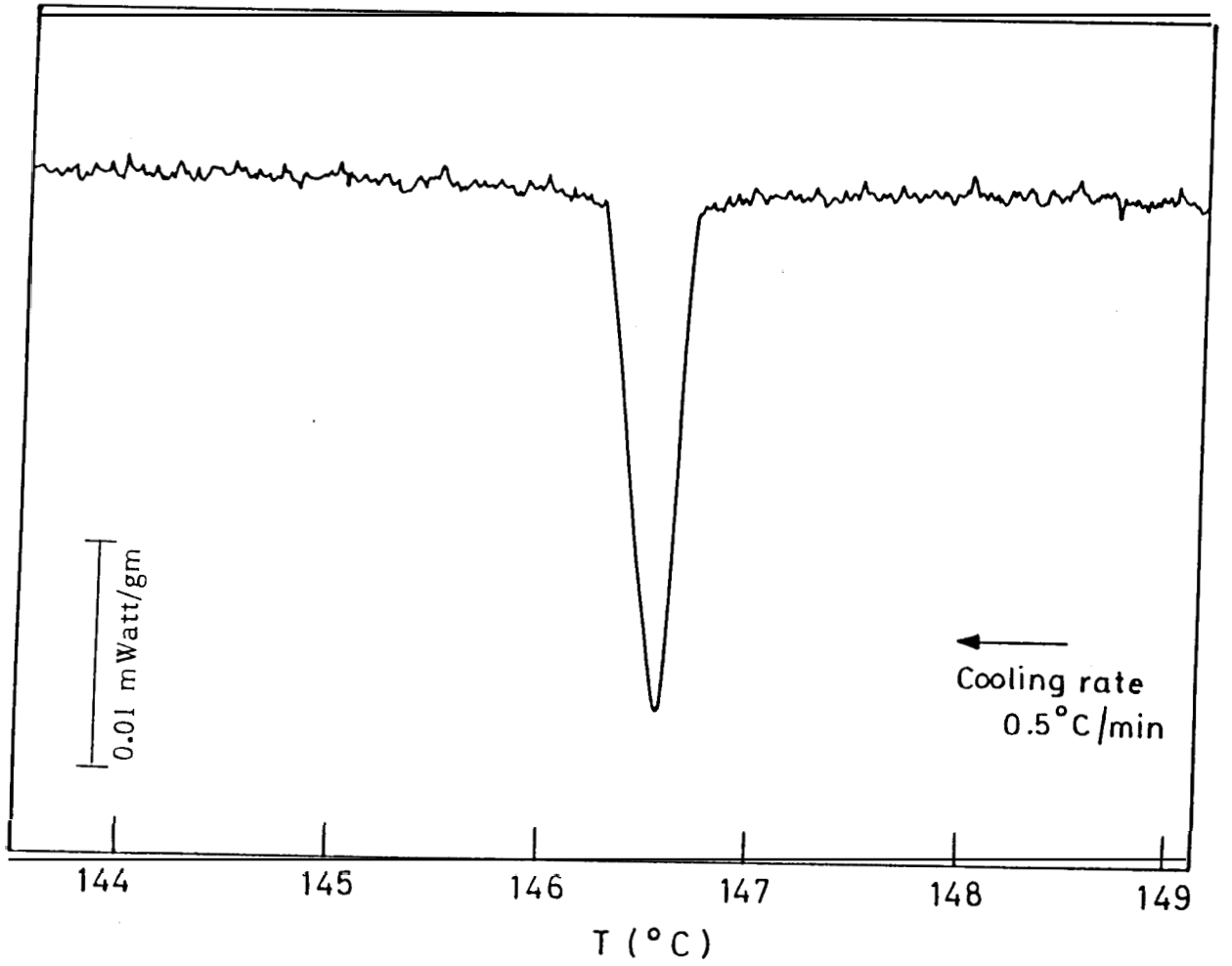

Figure 4.21. DSC run for 65.6% mixture of DB5 showing a strong signal at A_d-A_2 transition.

in the range of the A_d phase with increasing X so that instead of an A_d-A_2 critical point, an A_d-A_2-N point is observed. Although no detailed Xray measurements have been done on N-A_2 boundary, it is likely that this transition is first order. A_d-A_2 transition is also first order. Therefore assuming N-A_d transition as second order, an assumption which is justified in view of large nematic range for this concentration, the N-A_d line ends as a critical end point (C.E.P.). The topology of the phase diagram surrounding the critical end point is shown on enlarged scale in the Fig.4.22. It is seen that A_d-A_2 and N-A_2 boundaries are continuous through the NA_dA_2 point while NA_d approaches obliquely, a feature which perhaps indicates that it is a critical end point. Evidently further studies on NA_d and NA_2 boundaries are required before the existence of C.E.P. is established unambiguously.

Thus we have seen a clear A_d-A_2 transition in the T-X diagram of DB5/9OBCB system, the signature of which is seen as a coexistence region shown by Xray diffraction experiments with a pronounced jump in the layer spacing at the transition. However, the A_d-A_2 critical point was elusive in this binary system.

4.5 STUDIES ON 11OPCBOB-9OBCB BINARY SYSTEM

It was shown in the previous section that the T-X diagram of DB5/9OBCB gives an A_d-A_2 phase boundary which does not terminate at a gas-liquid type of a critical point. With a view to observe such a

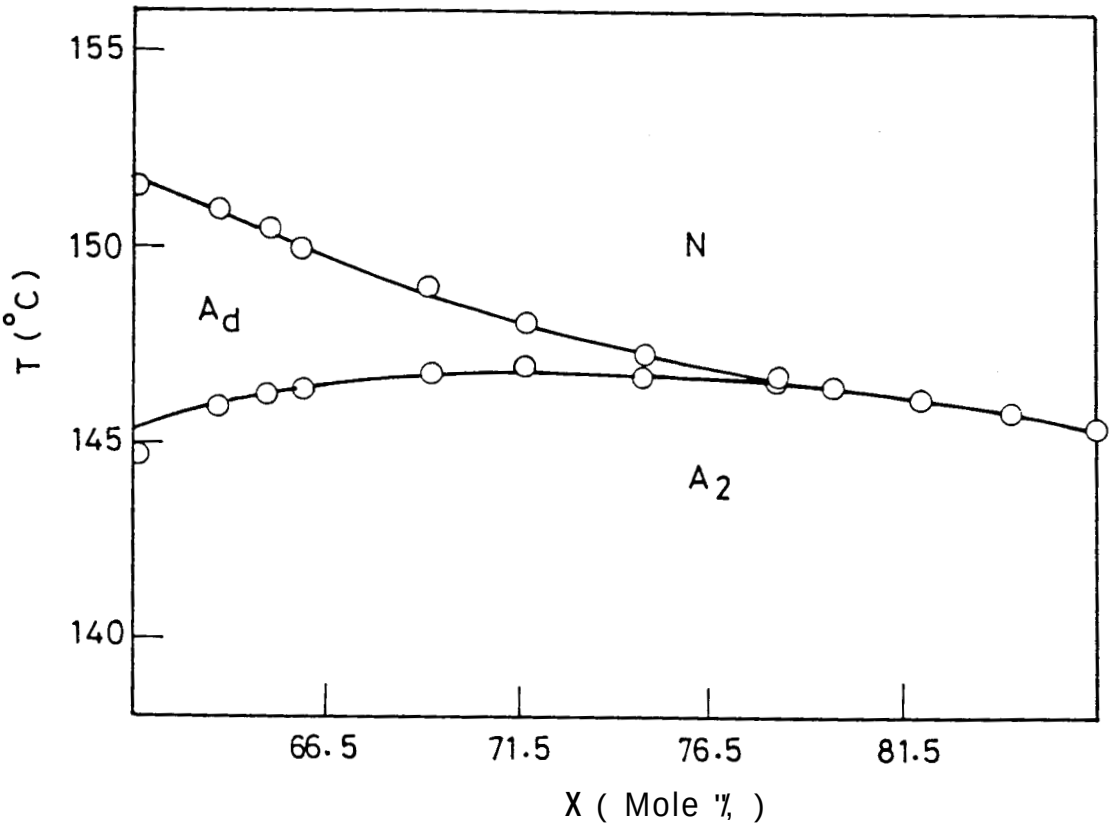

Figure 4.22

Detailed temperature-concentration diagram in the vicinity of critical end point. X is mol % of DB5.

critical point we proceeded to mix 9OBCB with 11OPCBOB (a compound for which A_d phase continuously evolves into an A_2 phase). This resulted in the observation of the A_d-A_2 critical point in the T-X diagram. We shall now discuss the results of these experiments in the following.

T-X diagram.

The structures of 11OPCBOB and 9OBCB are shown in the Figs. 4.10 and 4.13 respectively and transition temperatures are listed in the tables 4.1 (9OBCB) and 4.2 (11OPCBOB). 9OBCB is a tri-aromatic material with only one bridging dipolar group whose longitudinal component opposes the direction of the cyano end group. The 11OPCBOB material is also a triaromatic compound, but it has two ester linkage groups whose dipoles are disposed opposite to that of the cyano end group. 9OBCB exhibits nematic, smectic A_d and ribbon phases ($\tilde{C}$) while 11OPCBOB exhibirs nematic, smectic A_d and smectic A_2. As remarked earlier this compound was believed to exhibit an A_d-A_2 transition, but subsequent accurate Xray studies[22] showed that such a transition does not exist and the A_d phase evolves continuously into the A_2 phase. The complete phase diagram of 11OPCBOB and 9OBCB systems is shown in Fig.4.23. This phase diagram has been obtained on the basis of textures observed in a polarizing microscope. Several interesting features are observable from this phase diagram:-

i) With increasing concentration of 11OPCBOB, the range of

TABLE 42

Transition temperatures (in °C) of 11OPCBOB

Material	K	A_2	A_d	N	I
11OPCBOB	106		154.5	159.3	

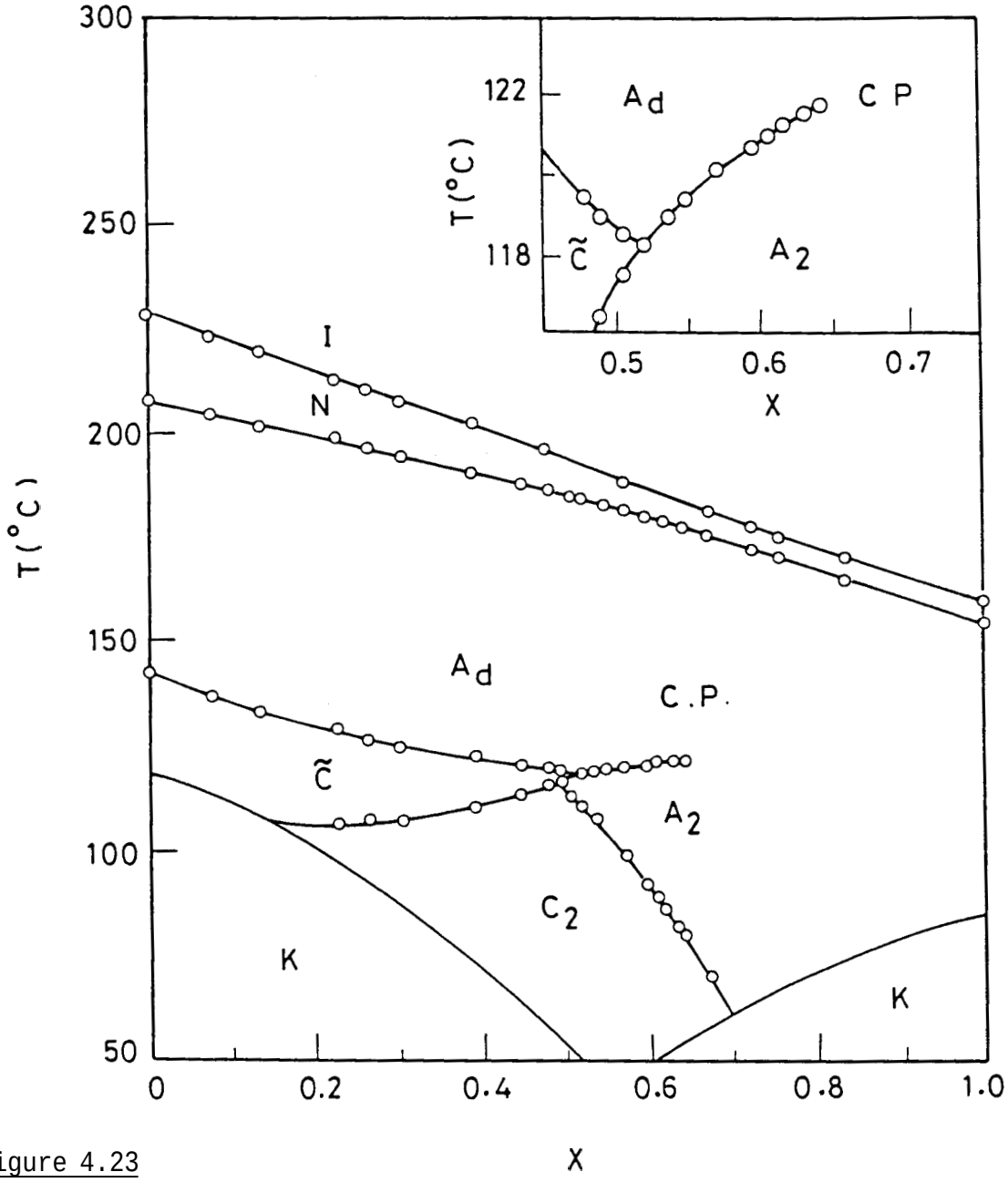

Figure 4.23

Temperature-concentration diagram for varying mole fraction of X of 11OPCBOB in the mixture. The first order transition line between A_d and A_2 phases terminates at the critical point (CP). The phase diagram in the vicinity of CP is shown in the inset on an enlarged scale. K : crystal, N : nematic, I : isotropic, $\tilde{C}$: tilted smectic A antiphase, and C_2 : bilayer C phase.

$\tilde{C}$ phase decreases resulting finally in the suppression of $\tilde{C}$ phase at X–0.52. This leads to a A_d, $\tilde{C}$, A_2 triple point.

ii) For concentration range $0.52 < x < 0.642$, a direct A_d-A_2 transition is seen beyond which the transition could not be observed optically. As in the case of DB5/9OBCB, the A_d-A_2 transition was clearly seen as a readjustment of a focal conic texture. Such a textural change could be seen regardless of rate of cooling or heating. For concentrations $X > 0.642$, no such textural changes between A_d and A_2 phases could be seen.

iii) A bilayer smectic C phase C_2 is observed for binary mixtures over a concentration range 0.2 to 0.7.

We shall. now describe the results of our Xray studies which have led to the first observation of A_d-A_2 critical point.

Xray Results

All the mixtures were freshly prepared and sharpness of the transition temperature was used as a measure of checking the homogeneity of mixing. The thoroughly mixed sample was taken into a Lindemann capillary whose ends were then sealed. The capillary with the sample was then loaded into a temperature controlled oven which in turn was placed between the pole pieces of an electromagnet of field strength 2.4 Tesla. The sample was heated to the nematic phase and cooled very slowly to the A_d phase in the presence of the field.

The strong magnetic field and the very slow rate of cooling adopted near nematic-smectic A_d transition ensured that the sample was very well aligned and that the degree of mosaicity of the alignment was also very favourable for Xray experiments. The sample was then cooled a few degrees below nematic-smectic A_d transition. The sample along with the temperature controlled oven was then transferred on to goniometer head of a computer controlled Guinier Xray diffractometer. Once the alignment of the sample was obtained in A_d phase, this alignment was retained even after removal from the magnetic field. The experimental details concerning the Xray diffractometer used have already been described in chapter II and only some relevant comments on the accuracy of the measurements will be made here. The K_{α_1} and K_{α_2} lines were separated using a bent quartz monochromator used in Johansson geometry and only K_{α_1} beam was used. A typical experiment was carried out in the following manner. An initial scan was taken (along the equatorial plane) by changing the position of the counter in steps of 0.01" and the approximate θ position of the diffraction peak was obtained. A refined θ scan was then taken around this θ position by moving the counter in steps of 0.001". The data were fitted to a second degree polynomial by using a least-squares-fit program. The value of θ obtained in this manner was used in the calculation of the layer spacing. The on-line θ refinement at any temperature required about 5 to 7 min. During this period the temperature of the sample was maintained to a constancy of ^{*10} mK. The

precision in the layer spacing measurement is better than ± 0.05 Å which corresponds to a precision in wavevector determination of 2×10^{-4}. The resolution in the z-direction (equatorial) is estimated to be 1.4×10^{-3}/Å. With this set up we have conducted detailed Xray studies on binary mixtures of concentrations, X = 0.55, 0.571, 0.597, 0.61, 0.642, 0.71 5, 0.8, and 1.0. The Xray diffraction pattern in the A_d phase was found to consist of quasi-Bragg peaks at wavevectors q_0' and $2q_0'$ while that in the A_2 phase showed peaks at q_0 and $2q_0$ (Fig.4.24). We also sometimes observed, depending on the mosaicity of the aligned sample, diffuse scattering centred around $2q_0$ in the A_d phase. The signature of the A_d-A_2 transition was a two-phase region whose diffraction pattern consisted of both q_0 and q_0' as well as the wavectors corresponding to the second harmonic (Fig. 4.24b). Fig. 4.25a-h gives the temperature variation of q_0 and q_0', the primary wavevectors in A_2 and A_d phases, for individual concentrations, X = 0.550, 0.571, 0.597, 0.619, 0.642, 0.715, 0.80 and 1.0 (11OPCBOB). Fig.4.26 shows a consolidated plot of the data for all these concentrations, restricted to a narrow range of temperature in the vicinity of the expected A_d-A_2 transition. For all $x < 0.642$ the A_d-A_2 transition is seen. Fig.4.25 also shows data in the two phase region (coexistence region). It is seen that the variations of q_0' and q_0 in this region are nothing but continuations of the trends in the variation of the wavevectors in the A_d and A_2 phases, so much so, we can associate a jump in the wavevector at the A_d-A_2 transition.

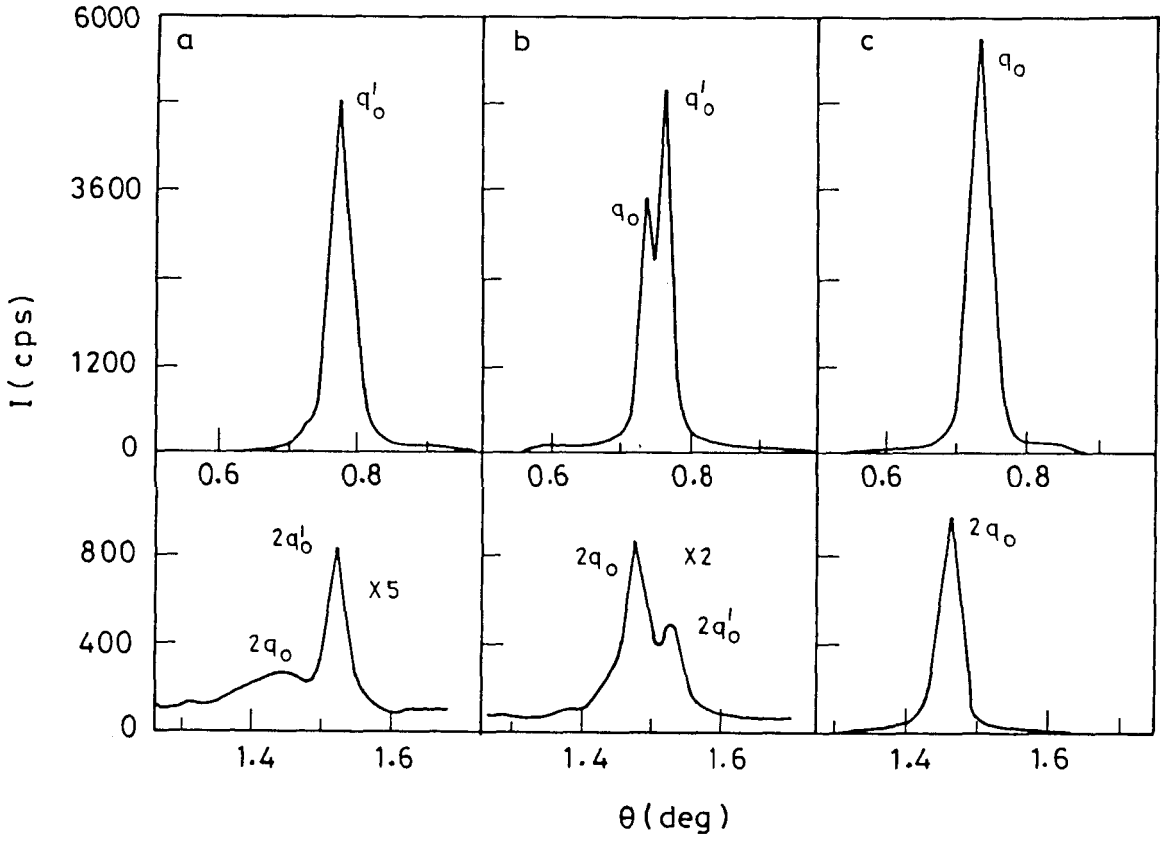

Figure 4.24

Raw diffractometer scans taken along the equatorial direction ($q_\perp = 0$) for the X = 0.608 mixture showing the Xray scattered intensity, I (counts per second) as a function of the scttering angle (θ). (a) A_d phase T = 121.5°C. The quasi-Bragg peaks are at q'_0 and $2q'_0$, the latter one is seen over-riding on the diffuse scattering centred around $2q_0$, (b) Two phase region (T = 121.1°C) showing the coexistence of q_0 and q'_0 as well as of $2q_0$ and $2q'_0$. (c) A_2 phase (T = 120.3°C) with the diffraction peaks at q_0 and $2q_0$, The intensities of the second harmonics in (a) and (b) have been multiplied by a factor 5 and 2 respectively.

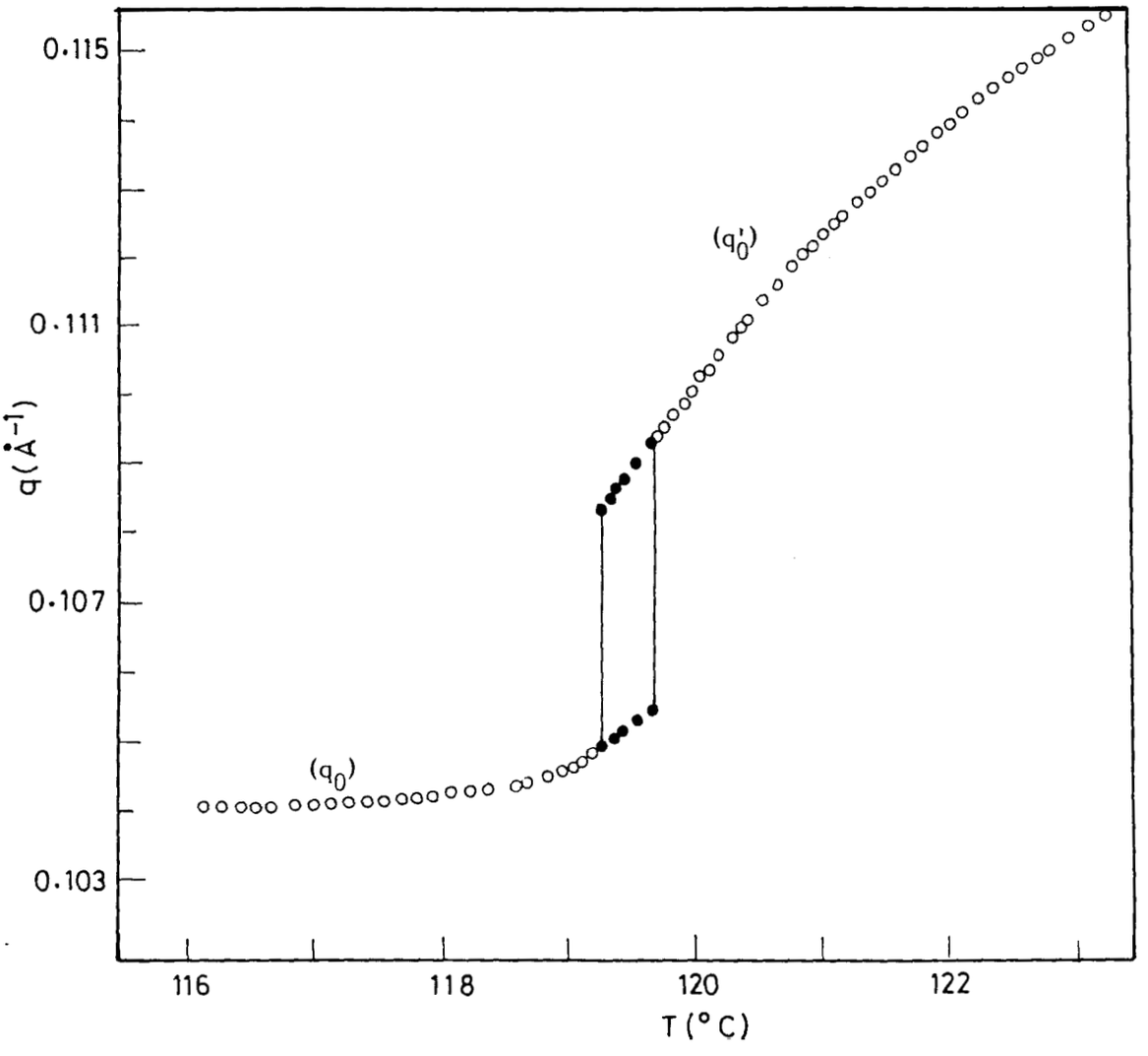

Figure 4.25(a)

Variation of wavevectors q_0 and q_0' vs. temperature (T) for binary mixture X = 0.55 (mol fraction of 11OPCBOB). The data in the two phase region are shown by closed circles and the vertical lines represent approximately the width of two phase region.

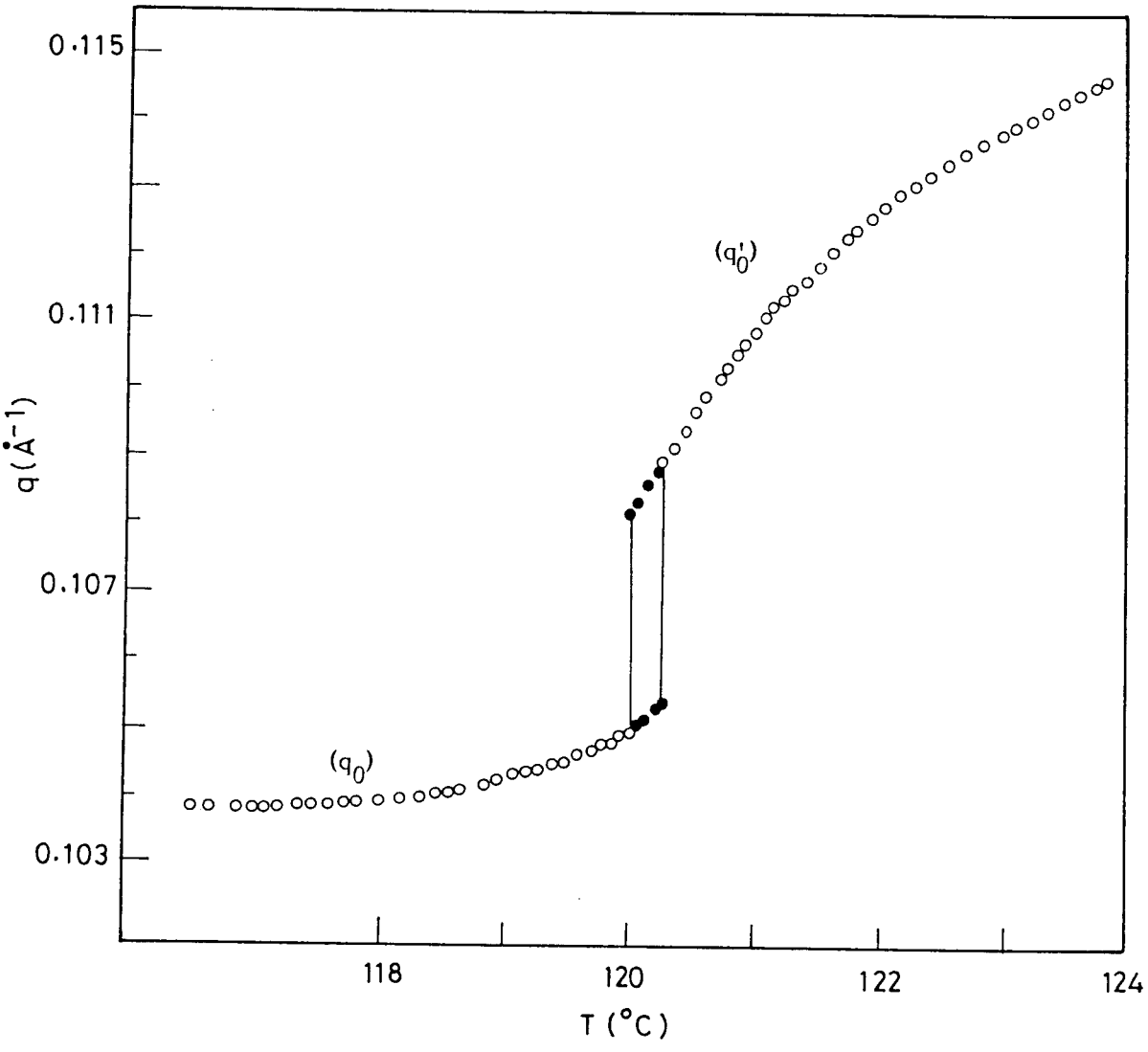

Figure 4.25(b)

Variation of wavevectors q_0 and q_0' vs. temperature (T) for binary mixture X = 0.571. See also legend of Fig. 4.25(a).

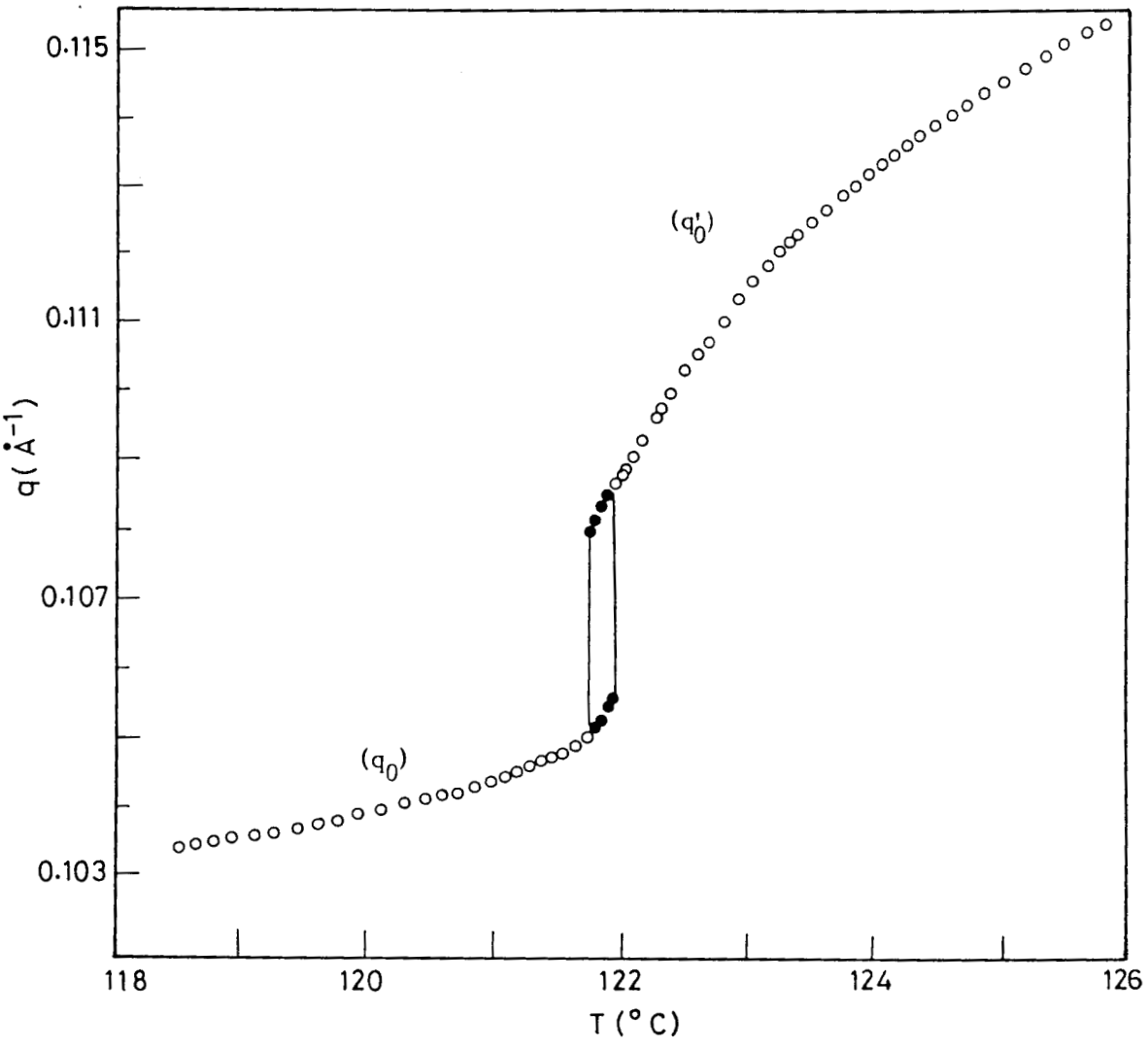

Figure 4.25(c)

Variation of q_0 and q_0' vs. temperature for X = 0.597. (See also legend of Fig. 4.25a)

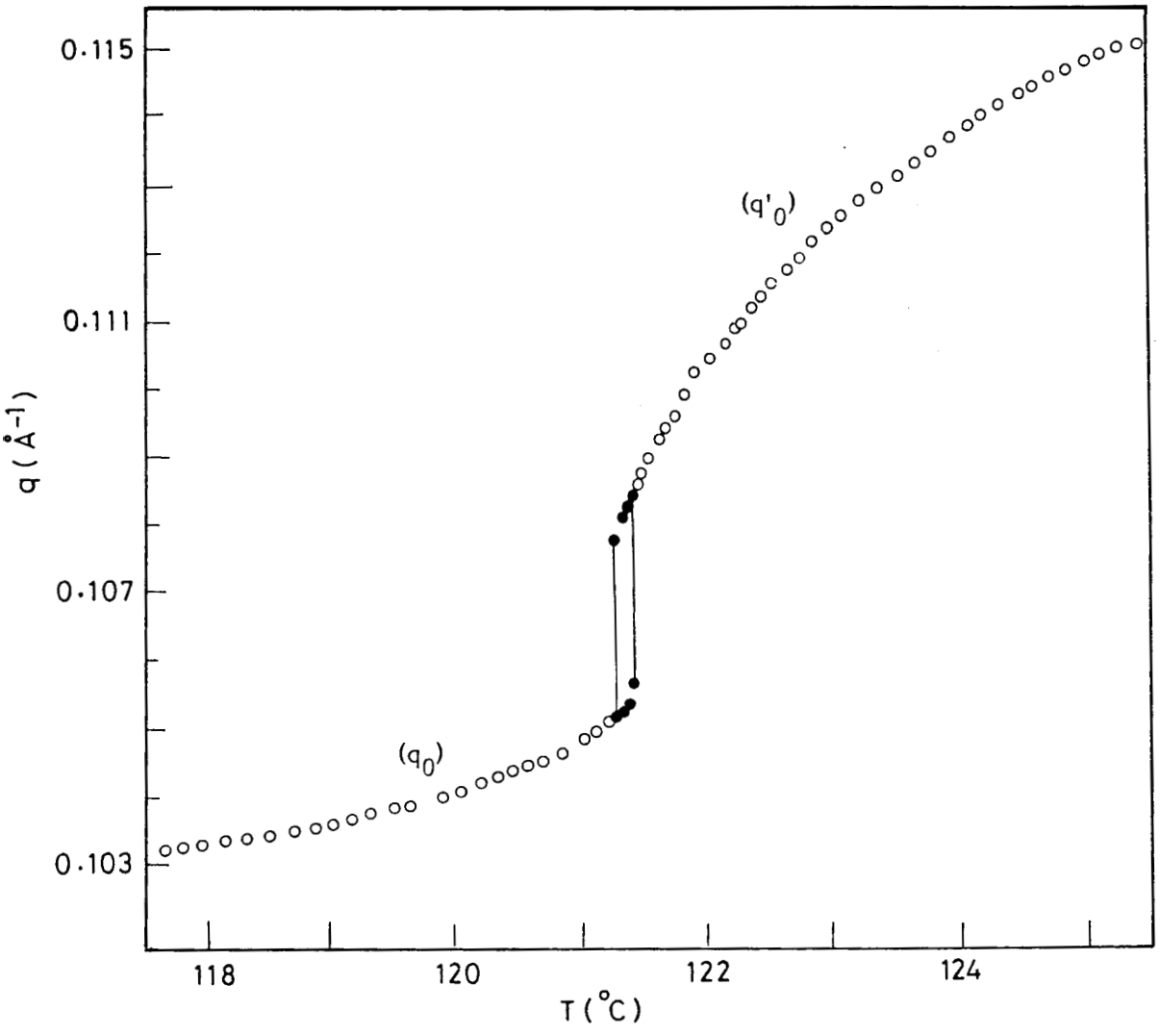

Figure 4.25(d)

Variation of q_0 and q_0' vs. temperature (T) for X = 0.619.
(See also legend of Fig. 4.25a)

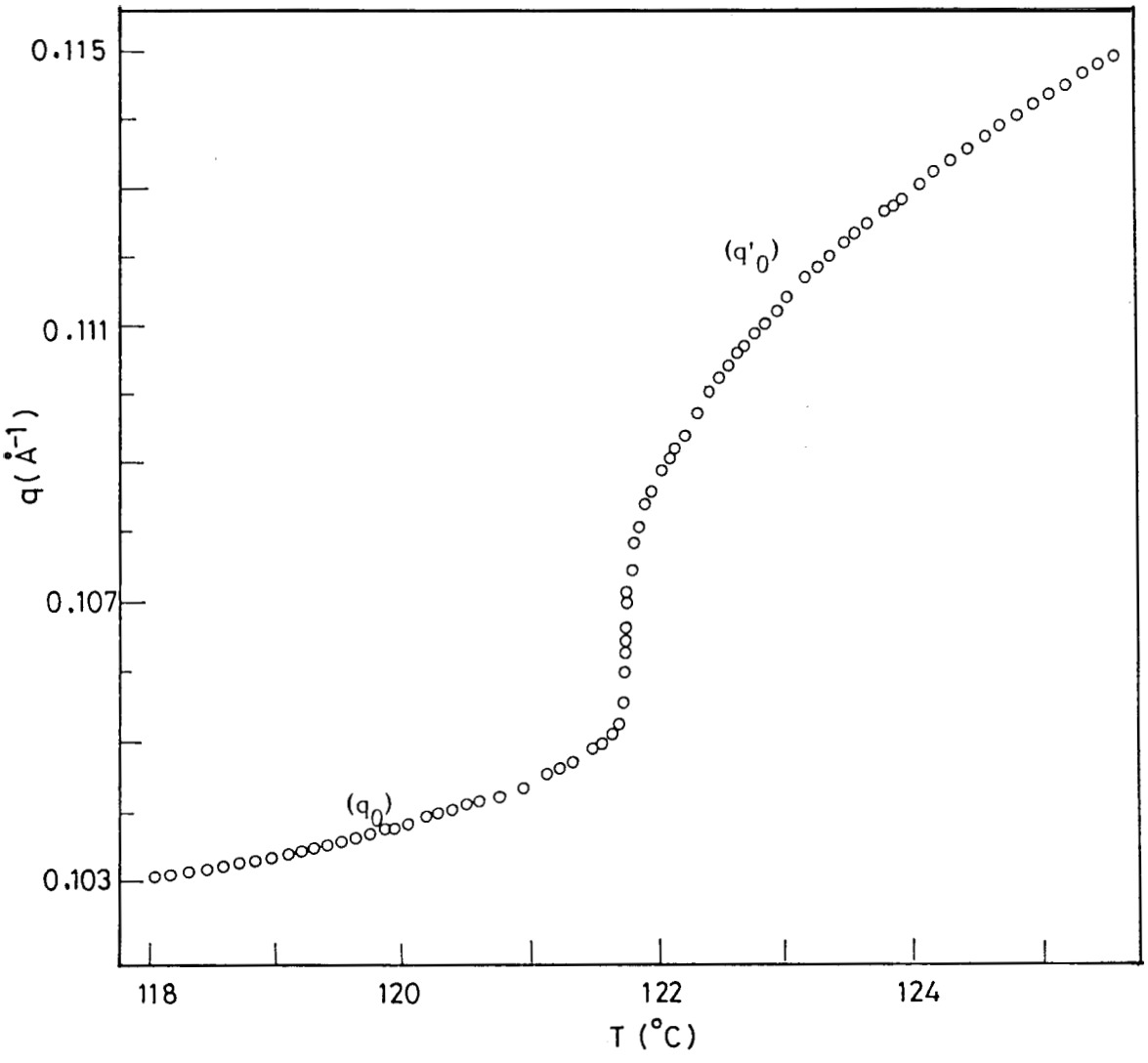

Figure 4.25(e)

Variation of q_0 and q_0' vs. temperature (T) for a binary mixture X = 0.642 mol fraction of 11 OPCBOB.

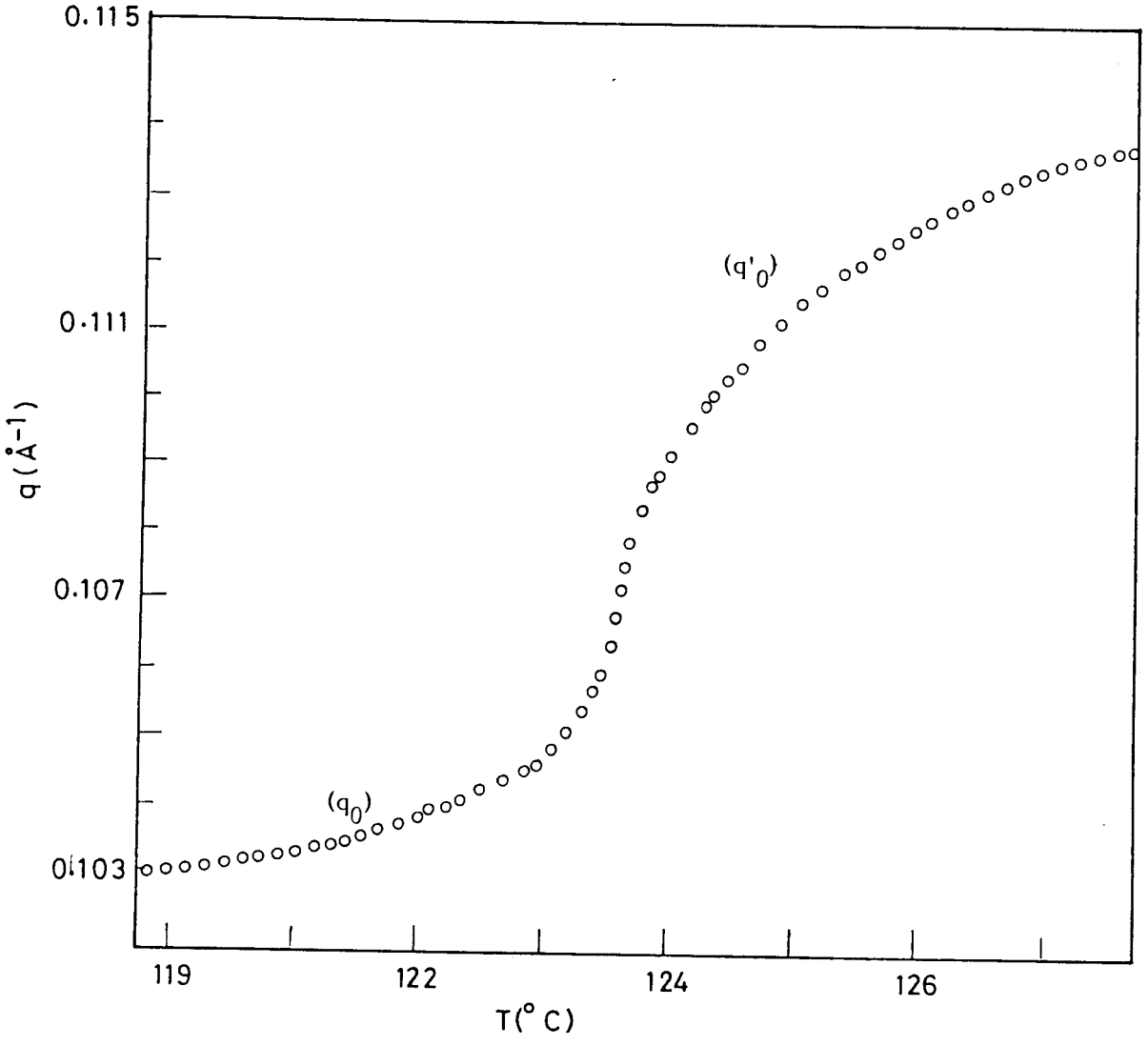

Figure 4.25(f)

Variation of q_0 and q_0' vs. temperature (T) for mixture X = 0.715 mol **fraction of** 11OPCBOB.

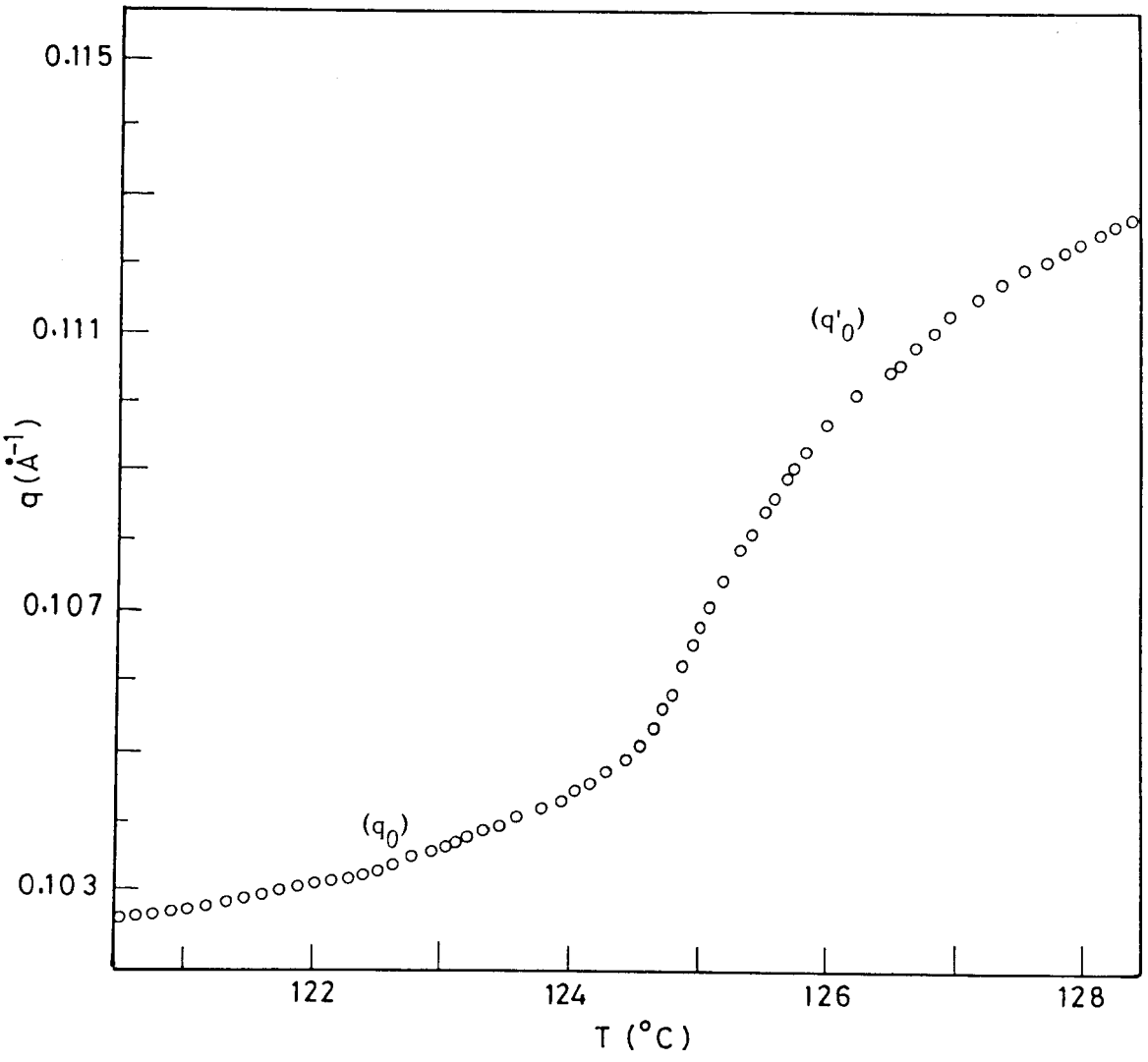

Figure 4.25(g)

Variation of q_0 and q_0' vs. temperature (T) for binary mixture X = 0.80 mol fraction of 11OPCBOB.

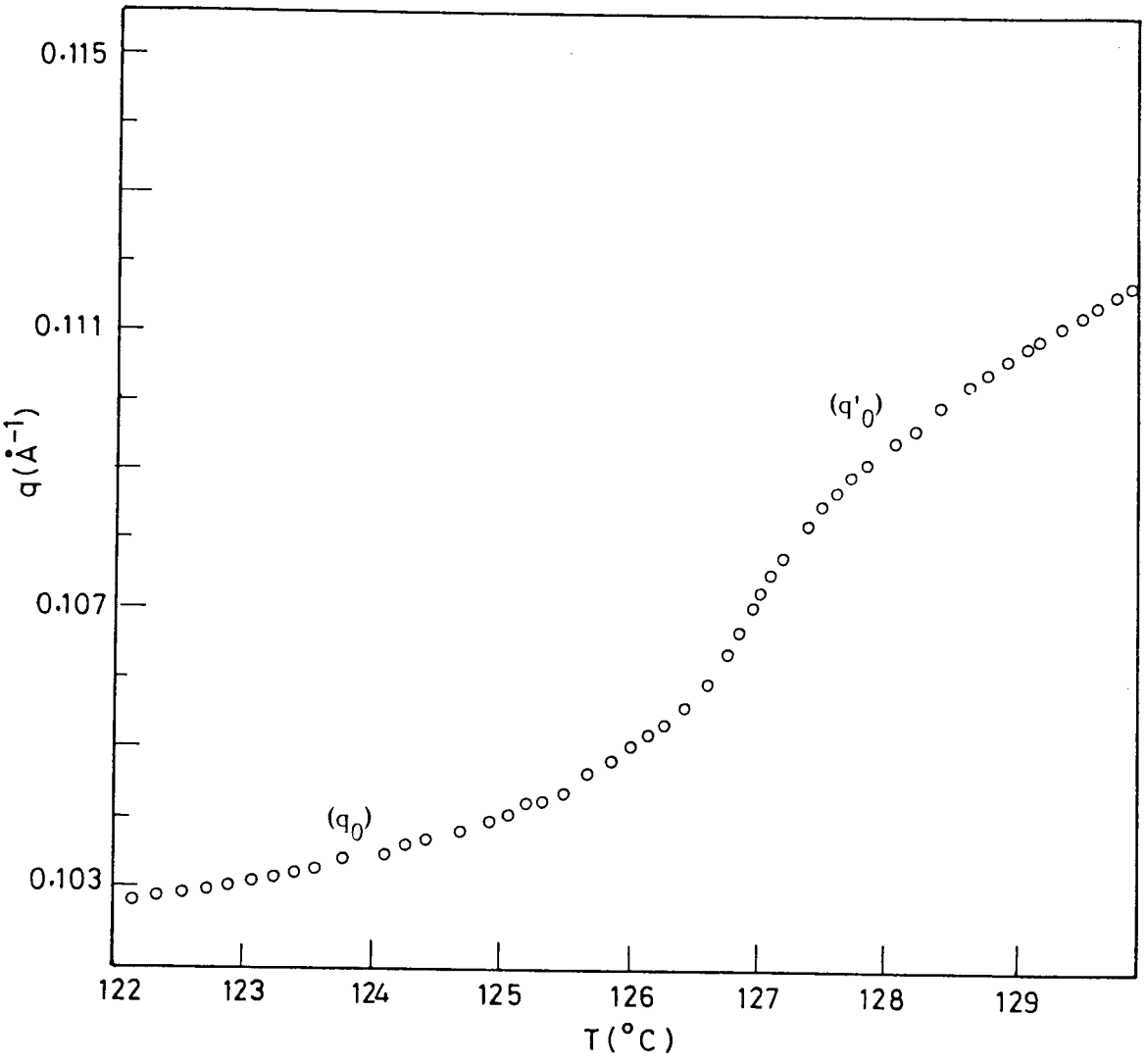

Figure 4.25(h)

Variation of q_0 and q_0' vs. temperature for 11OPCBOB.

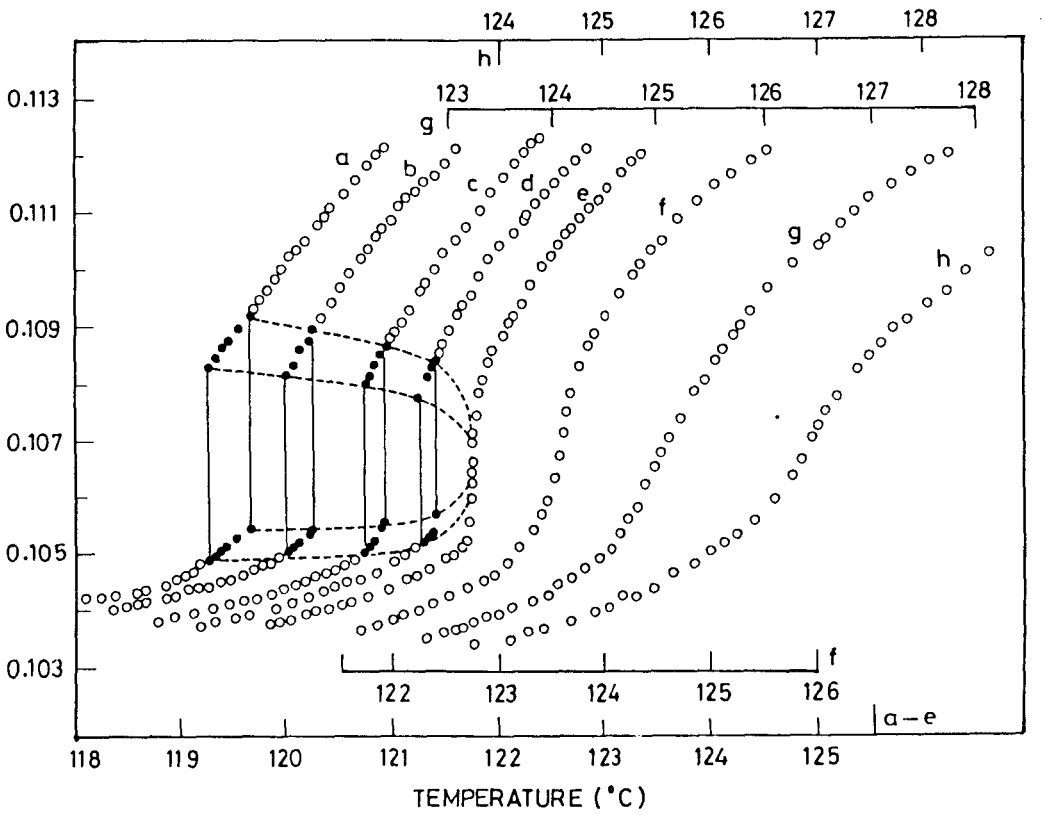

Figure 4.26

Plot of wavevectors q_0 and q_0' vs. temperature (T) for different mixtures of 11OPCBOB/9OBCB. The mole fraction (X) of 11OPCBOB in the mixtures are (a) 0.55, (b) 0.571, (c) 0.597, (d) 0.619, (e) 0.642, (f) 0.715, (g) 0.80 and (h) 1.0 or 11OPCBOB. The corresponding temperature scales are identified. The data in two phase region are shown as closed circles while the vertical lines represent. the approximate width of this region. The dashed lines are envelopes of the ends of the two-phase regions and are only guides to the eye. The critical point (CP) is identified by the vertical inflexion point seen for X = 0.642 (plot e).

It is seen from Fig.4.25a-d that the magnitude of the wave-vector jump is about 0.0034 $\mathring{A}^{-1}$ for X=0.55, 0.0032 - for X=0.571, 0.003 $\mathring{A}^{-1}$ for X=0.597 and 0.0025/$\mathring{A}^{-1}$ for X=0.619 and the corresponding coexistence regions being 0.41°C, 0.25°, 0.21°, 0.14°C respectively. It is clear that the magnitude of the wavevector jump decreases with increasing X with an accompanying decrease in the width of the two-phase region, until at X=0.642, no jump is seen within the resolution of our experimental set up. Instead, a 'vertical inflection point' is observed for this concentration. For X > 0.642, the wavevector q_0' evolves continuously into q_0 without any jump. The inflection point becomes less pronounced on approaching 11OPCBOB (i.e., X > 0.642). All these features - the shrinking of the two phase coexistence region associated with the first order A_d-A_2 transition and the accompanying decrease in the difference between q_0 and q_0' at the transition, the vertical inflection point becoming less pronounced for x > 0.642 - are clearly indicative of rhe existence of a critical point at X=0.642. For higher values of X, A_d phase evolves continuously into an A_2 phase without a phase transition. Thus we have observed that two smectic A phases (A_d and A_2) with different layer periodicities can coexist along a line of first order transition terminating at a critical point beyond which the distinction between the two phases ceases to exist. It is also seen that our consolidated q-T plot (Fig.4.26) is strikingly similar to the q-T plot predicted theoretically[14] (Fig. 4.8).

So far, we presented the data concerning the wavevectors q_0 and q_0'. As remarked earlier the Xray diffraction pattern in the A_d phase consisted of quasi Bragg peaks at wavevectors q_0' and $2q_0'$. In addition a diffuse scattering is centred around $2q_0$ in the A_d phase. In the case of an A_2 phase the diffraction peaks were found at q_0 and $2q_0$ positions. Although it was easy to identify the peak at $2q_0$ in A_2 phase, the 2qb peak in A_d phase was much more difficult to detect since the relative strengths of the peak at $2q_0'$ with respect to that at q_0' peak was extremely small (<1%) compared to relative strengths of q_0 and $2q_0$ (10%) in A_2 phase. For this reason it was not always possible to follow the $2q_0'$ peak as a function of temperature for all concentrations. Also, the problem caused by the close proximity of diffuse $2q_0$ modulation affected the accuracy in the determination of $2q_0'$. Considering these factors the data for 2qb do not have the same precision as that of q_0. Nevertheless we have shown the data corresponding to $2q_0'$ and $2q_0$ as a function of temperature for different concentrations X = 0.55, 0.571, 0.597, 0.619. 0.71 5 and 11OPCBOB in Fig.4.27a-f. Clearly these plots show the same features as shown by the fundamental wavevectors.

Calorimetric Studies

It is well known from studies on binary liquid mixtures[24] that the specific heat fluctuations build up as the critical point is approached from the critical region side. In order to see if such an effect

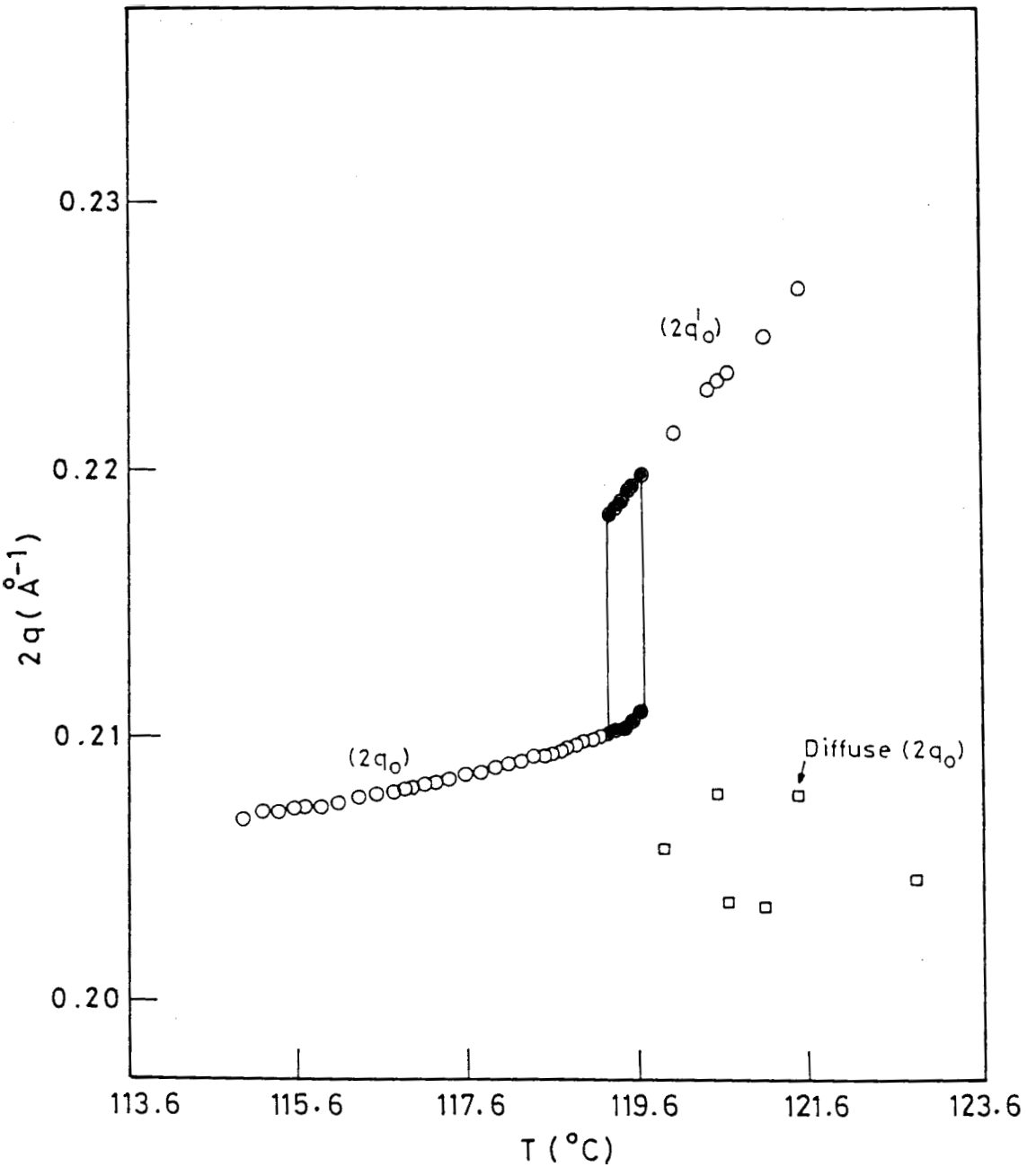

Figure 4.27(a)

Plot of $2q_0$ and $2q'$ vs. temperature (T) for mixture X = 0.55 mol fraction. The data in the two-phase region are shown by closed circles and the region between the vertical lines represents approximately the width of the two-phase region.

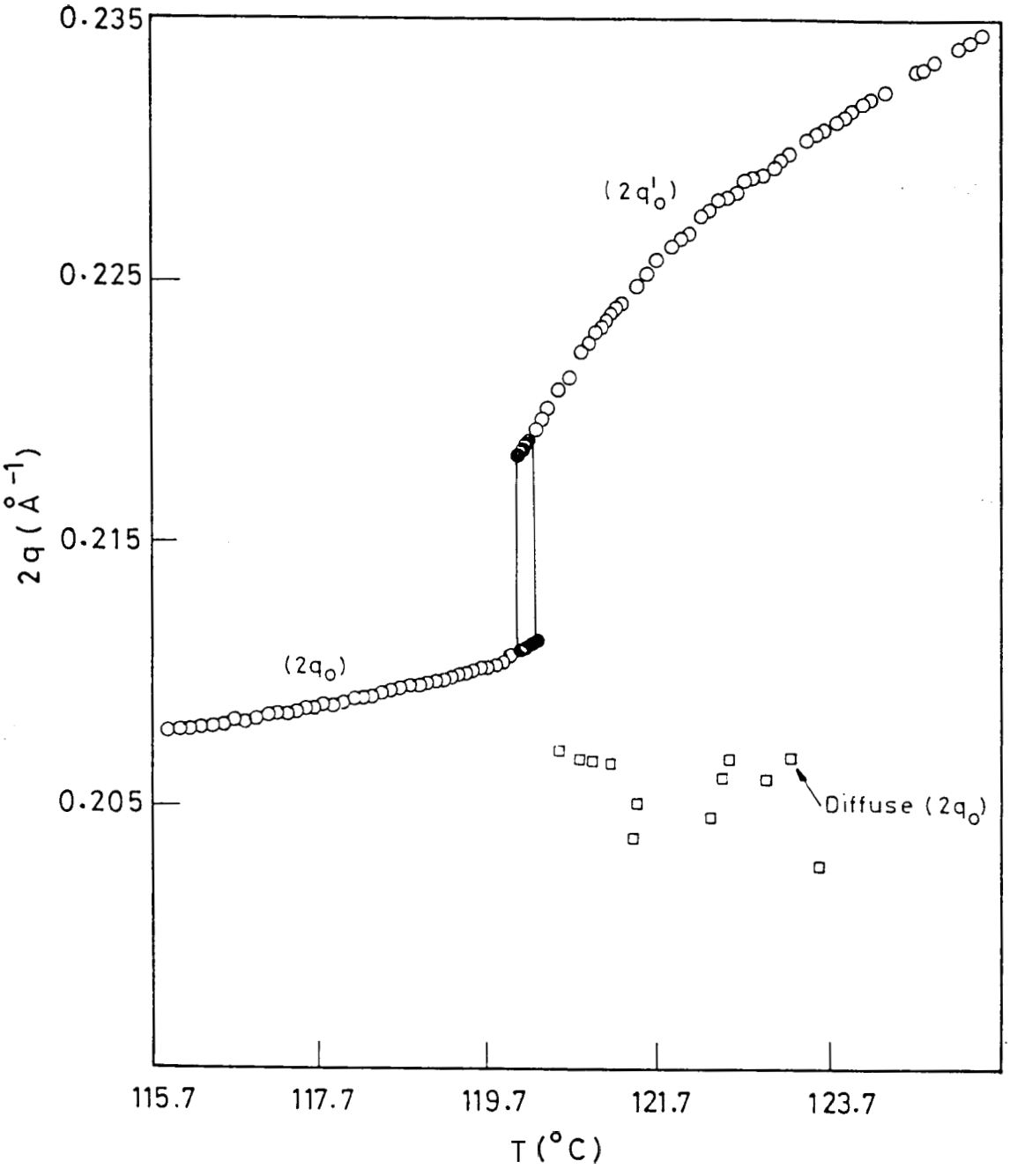

Figure 4.27(b)

Plot of $2q_0$ and $2q_0'$ vs. temperature (T) for mixture X = 0.571. (See also legend of Fig. 4.27a).

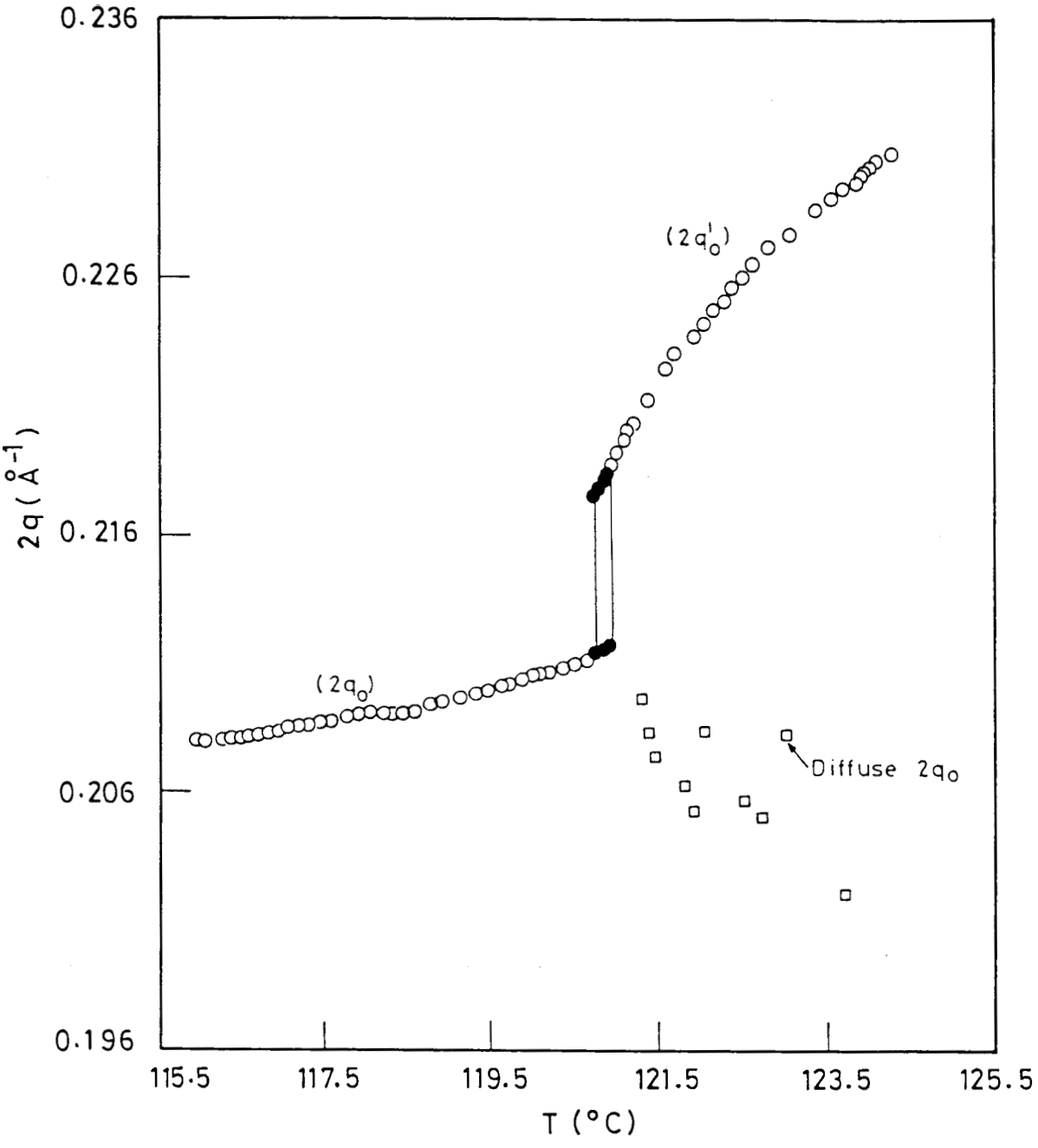

Figure 4.27(c)

Plot of $2q_0$ and $2q_0'$ vs. temperature (T) for X = 0.597. *(See* also legend of Fig. 4.27a).

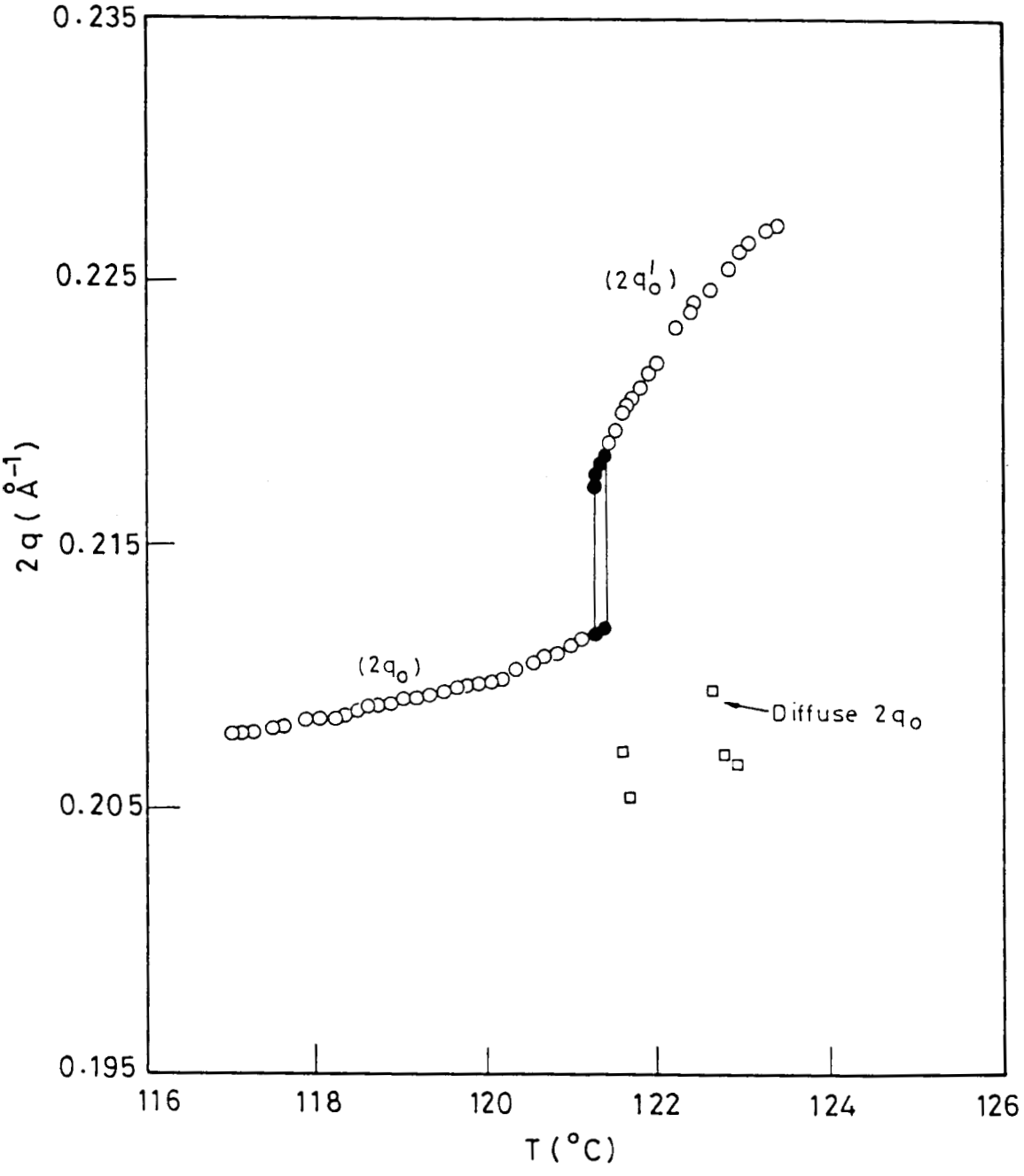

Figure 4.27(d)

Plot of $2q_0$ and $2q'_0$ vs. temperature (T) for mixture X = 0.619. (See also legend of Fig. 4.27a).

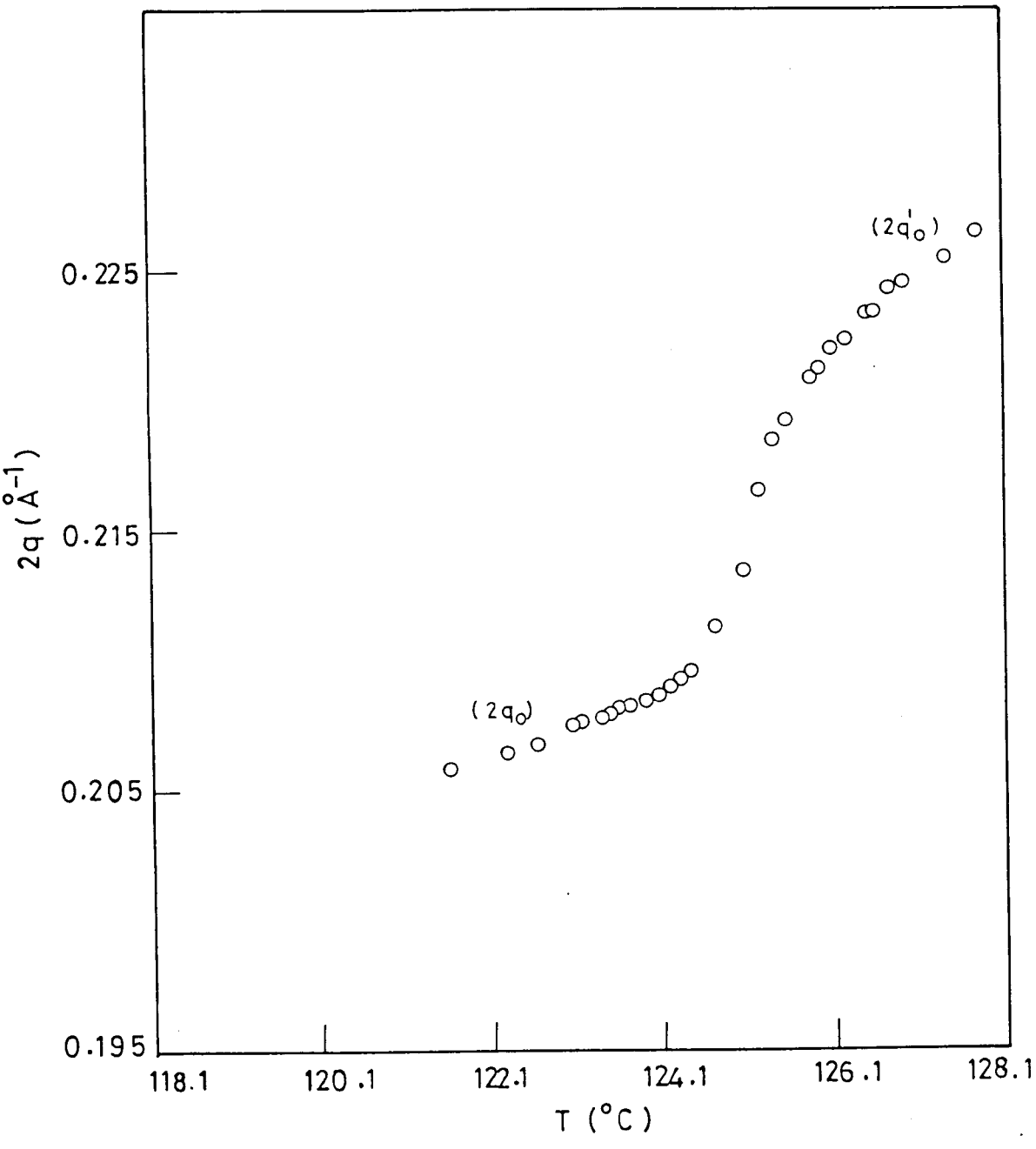

Table 4.27(e)

Plot of $2q_o$, $2q'_o$ versus temperature (T) for mixture X = 0.715 (mol. fraction)

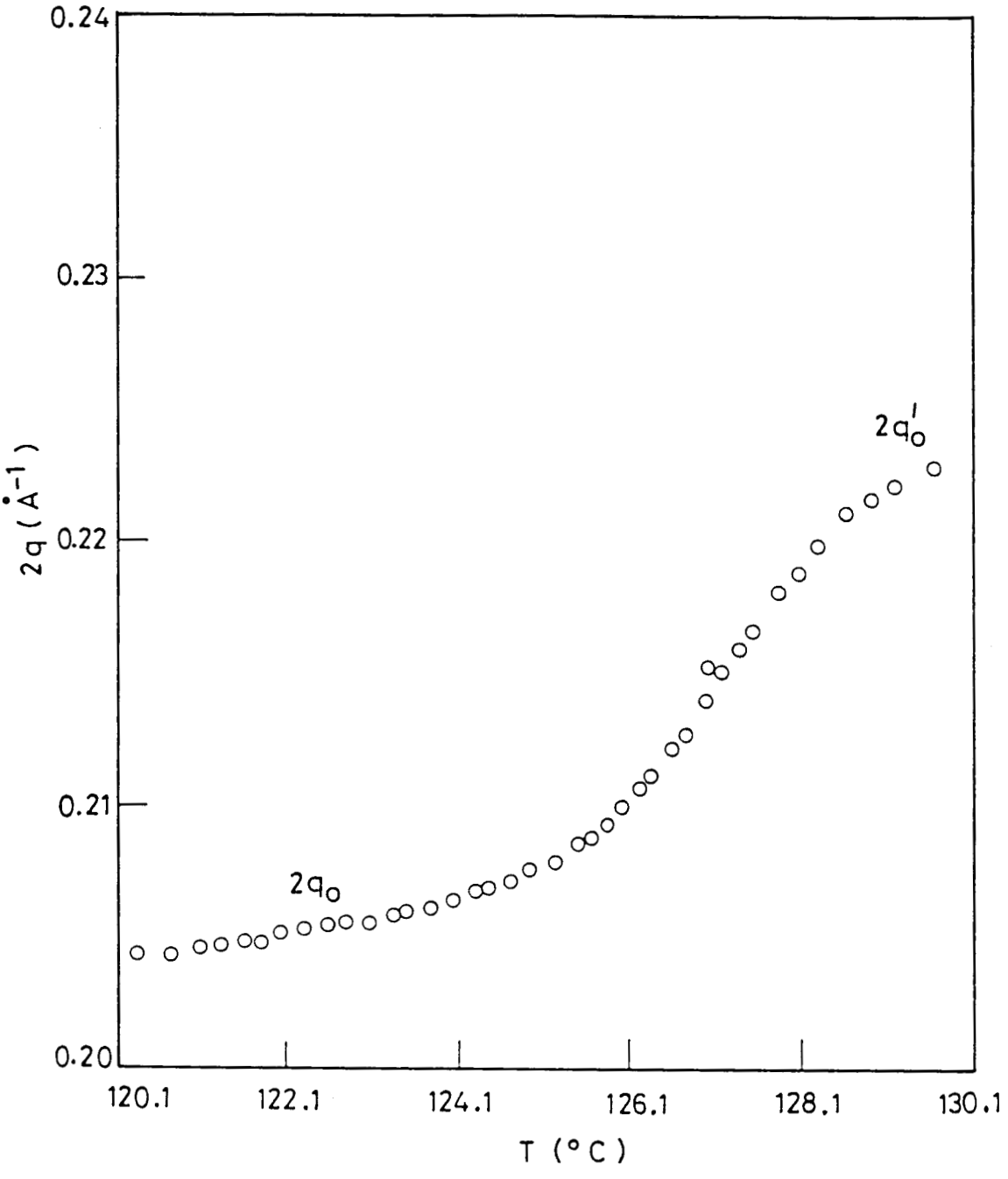

Figure 4.27(f)

Plot of $2q_0$ and $2q_0'$ vs. temperature (T) for 11OPCBOB.

can be seen at least qualitatively in our system, we have taken DSC runs for four concentrations, viz., 1.0, 0.715, 0.673 and 0.652, all of which lie in the critical region, i.e., the region where A_d phase evolves into an A_2 phase continuously without a phase transition. These raw runs are shown in Fig.4.28. (All these runs were taken under identical experimental conditions - nearly the same quantity of the material taken in the DSC cups, same rate of heating or cooling was adopted after equilibriating the sample for same period of time). It is seen that for X=1.0, the run (Fig. 4.28a) shows only a small peak. But as $X_{c.p.}$ is approached the strength of the DSC signal increases and also the signal gets sharper. It is interesting to note that calorimetry shows a peak even for concentrations far away from $X_{c.p.}$ In the absence of the Xray data, these calorimetric results could have been wrongly interpreted as indicating A_d-A_2 transition. As discussed, however, our Xray studies show that for all the four systems there is no A_d-A_2 transition, but only a continuous evolution of A_2 from A_d. Interestingly, the temperature at which the DSC runs show a peak corresponds to the point of inflection in the q-T plots. It is thus seen that as $X_{c.p.}$ is approached the strength of this 'spurious' DSC signal increases indicating the increase of specific heat fluctuations. It is relevant to recall here that recent high resolution AC calorimetric studies[25] on DB7OCN, a compound which also shows a continuous evolution of A_d phase into A_2 phase, shows a strong specific heat signal, but with a rounding at the top. Thus the DSC

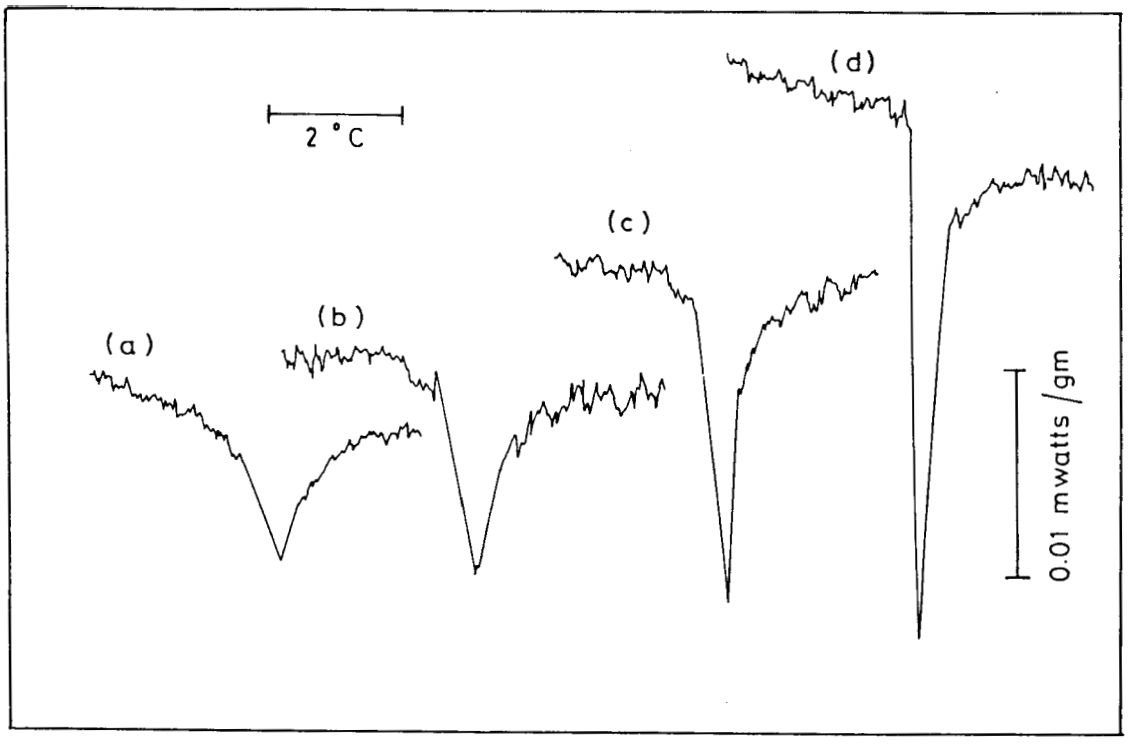

Figure 4.28

DSC runs for (a) 110PCBOB, (b) X = 0.715, (c) X = 0.673, and (d) X = 0.652 systems, taken at 0.5°C/min. cooling rate. The strength of the signal increases as CP is approached.

results show albeit qualitatively that there is an increase of specific heat effect as the critical point is approached. Clearly high resolution studies are required to analyse quantitatively the pre-transitional behaviour near critical point.

4.6 RECENT THEORETICAL STUDIES OF A_d-A_2 CRITICAL POINT

As remarked in preceding sections (4.2) the phenomenological theory, in the framework of mean field approach. predicts the existence of the A_d-A_2 critical point. Recently, Park et al.[26] have developed a more rigorous approach, i.e., a model nonlinear elastic Hamiltonian to describe the behaviour of different physical properties in the vicinity of the critical point (C). This theoretical study has been carried out using several approaches, viz., the mean field theory, one-loop order perturbation theory and the ε-expansion. The mean-field theory for this model is identical to the mean-field theory for the liquid-gas transition. In one-loop perturbation theory, critical corrections to the compressibility become important below an upper critical dimension of 6. In addition, there are important critical corrections to a third order vertex function between 6 and 8 dimensions indicating deviations from mean-field behaviours below 8 dimensions. They determined a fixed point in 6-E dimensions describing the critical point and calculated critical exponents to a first order in ε . This fixed point exhibits anisotropic scaling with different correlation length exponents $y_{\|}$ and $y_{\perp}$ parallel and perpendicular to the director. Scaling

properties and Xray scattering patterns in the vicinity of the S_{A_2}-S_{A_d} critical point are also considered. The approach of Park et al. leads to a number of theoretical predictions which should be valid in the vicinity of the A_2-A_d critical point in 3 dimensions. The most salient prediction is that the compressional elastic constant ($\bar{B}$) should vanish at the critical point in exact analogy with divergence of the bulk compressibility at the liquid-gas critical point. Although preliminary experiments[27] seemed to show a pronounced dip in $\bar{B}$ in the vicinity of the critical point, no exponents have yet been evaluated. The second theoretical prediction is that the specific heat at constant pressure (C_p) as well as $\bar{B}$ measured along the critical pressure line should yield an exponent ν/Δ. Consequently the product $C_p.\bar{B}$ is expected to be independent of temperature as the critical point is approached. Another interersting prediction of the theory is that C_p measured at constant layer spacing should have a singularity with characteristic exponent α. All these predictions are to be experimentally verified.

In conclusion, the experiments described in this chapter have proved the existence of A_d-A_2 critical point in the temperature-concentration plane. The strongest experimental evidence of its existence is the decrease in the discontinuity of the wavevector (Δq_0) at the A_d-A_2 transition with an accompanying decrease in the two-phase region as the critical point is approached. The existence of such a critical point is explainable on the basis of mean-field theory as well as fluctuation corrected theory. Evidently, further high resolution

experiments near the critical point are needed before the nature of this critical point is fully elucidated. A theoretical calculation of both the shape of the coexistence curve and the functional form Δq_0 would also be of considerable interest.

REFERENCES

1 N.V.Madhusudana and S.Chandrasekhar, Pramana, Suppl. I, p. 57 (Proc. Int. Liquid Crystals Conf., Bangalore, 1973).

2 A.J.Leadbetter, R.M.Richardson and C.N.Colling, J.de Phys., 36, Cl-37 (1975).

3 G.Sigaud, F.Hardouin, M.F.Achard, H.Gasparoux, 3. de Phys. Colloq., 40, C3-356 (1979).

4 F.Hardouin, A.M.Levelut, J.J.Benattar, G.Sigaud, Solid State Comrnun., 33, 377 (1980).

5 G.Sigaud, F.Hardouin, M.F.Achard and A.M.Levelut, J.de Phys., 42, 107 (1981).

6 A.M.Levelut, J.de Phys. Lett., 45, L-603 (1984).

7 B.R.Ratna, R.Shashidhar and V.N.Raja, Phys.Rev.Lett., 55, 1476 (1985).

8 J.Prost and P.Barois, J.Chim.Phys., 80, 65 (1983).

9 J.Wang and T.C.Lubensky, J.de Phys., 45, 1653 (1984).

10 P.G.de Gennes, The Physics of Liquid Crystals (Clarendon, Oxford, 1974).

11 J. Prost, J.de Phys., **40**, 581 (1979).

12 J. Prost, in "Liquid Crystals of One- and Two-dimensional Order", Ed. by W.Helfrich and G.Heppke (Springer-Verlag, Berlin, 1980), p.125.

J. Prost, in "Symmetries and Broken Symmetries in Condensed Matter Physics", Ed. N.Boccara (IDSET, Paris, 1981), p.159.

P. Barois, J. Prost and T.C.Lubensky, J.de Phys., 46, 391 (1985)

For a review, see F. Hardouin, A.M.Levelut, M.F.Achard, G.Sigaud, J. Chim. Phys., 80, 53 (1983)

K.K.Chan, P.S.Pershan, L.B.Sorensen and F.Hardouin, Phys.Rev. Lett., 54, 1694 (1985).

K.K.Chan, P.S.Pershan and F.Hardouin, Phys. Rev., A34, 1420 (1986).

F.Hardouin, Nguyen Huu Tinh, M.F.Achard and A.M.Levelut, J.de Phys. Lett., 43, L-327 (1982).

F.Hardouin, M.F.Achard, C.Destrade and Nguyen Huu Tinh, J.de Phys., 45, 765 (1984).

F.Hardouin, M.F.Achard, Nguyen Huu Tinh and G.Sigaud, J.de Phys. Lett., **46,** L-123 (1985).

F.Hardouin, A.M.Levelut and G.Sigaud, J. de Phys., 42, 71 (1981)

S. Krishna Prasad, R.Shashidhar, B.R.Ratna, B.K.Sadashiva, G.Heppke and S.Pfeiffer, Liquid Crystals, 2, 111 (1987).

P.S.Pershan, G.Appeli, J.D.Litster and R.G.Birgeneau, Mol. Cryst.Liq.Cryst., 67, 205 (1981).

24 A.Kumar, H.R.Krishna Murthy and E.S.Rajagopal, Physics Reports (Review Section of Physics Letters), **98,** 57 (1983).

25 C.W.Garland, C.Chiang and F.Hardouin (to be published).

26 Y.Park, T.C.Lubensky, P.Barois and J.Prost, Presented at the A.P.S. Meeting, New York, March 1987.

27 P.Barois, These d' Etat N d' Ordre 875, Bordeaux (1986).